Turbulent Burning Rates of

Near-Flammability-Limit H_2-Air-Steam Mixtures

by
Janet V. Loesel Sitar

A thesis submitted to the Faculty of Graduate Studies in
partial fulfilment of the requirements for the Degree of

Master of Science

Department of Mechanical and Industrial Engineering
University of Manitoba
Winnipeg, Manitoba

Canada

Name _____

Dissertation Abstracts International is arranged by broad, general subject categories. Please select the one subject which most nearly describes the content of your dissertation. Enter the corresponding four-digit code in the spaces provided.

Mechanical Engineering
SUBJECT TERM

| 0 | 5 | 4 | 8 |

SUBJECT CODE

U·M·I

Subject Categories

THE HUMANITIES AND SOCIAL SCIENCES

COMMUNICATIONS AND THE ARTS
Architecture 0729
Art History 0377
Cinema 0900
Dance 0378
Fine Arts 0357
Information Science 0723
Journalism 0391
Library Science 0399
Mass Communications 0708
Music 0413
Speech Communication 0459
Theater 0465

EDUCATION
General 0515
Administration 0514
Adult and Continuing 0516
Agricultural 0517
Art 0273
Bilingual and Multicultural 0282
Business 0688
Community College 0275
Curriculum and Instruction 0727
Early Childhood 0518
Elementary 0524
Finance 0277
Guidance and Counseling 0519
Health 0680
Higher 0745
History of 0520
Home Economics 0278
Industrial 0521
Language and Literature 0279
Mathematics 0280
Music 0522
Philosophy of 0998
Physical 0523

Psychology 0525
Reading 0535
Religious 0527
Sciences 0714
Secondary 0533
Social Sciences 0534
Sociology of 0340
Special 0529
Teacher Training 0530
Technology 0710
Tests and Measurements 0288
Vocational 0747

LANGUAGE, LITERATURE AND LINGUISTICS
Language
    General 0679
    Ancient 0289
    Linguistics 0290
    Modern 0291
Literature
    General 0401
    Classical 0294
    Comparative 0295
    Medieval 0297
    Modern 0298
    African 0316
    American 0591
    Asian 0305
    Canadian (English) 0352
    Canadian (French) 0355
    English 0593
    Germanic 0311
    Latin American 0312
    Middle Eastern 0315
    Romance 0313
    Slavic and East European 0314

PHILOSOPHY, RELIGION AND THEOLOGY
Philosophy 0422
Religion
    General 0318
    Biblical Studies 0321
    Clergy 0319
    History of 0320
    Philosophy of 0322
Theology 0469

SOCIAL SCIENCES
American Studies 0323
Anthropology
    Archaeology 0324
    Cultural 0326
    Physical 0327
Business Administration
    General 0310
    Accounting 0272
    Banking 0770
    Management 0454
    Marketing 0338
Canadian Studies 0385
Economics
    General 0501
    Agricultural 0503
    Commerce-Business 0505
    Finance 0508
    History 0509
    Labor 0510
    Theory 0511
Folklore 0358
Geography 0366
Gerontology 0351
History
    General 0578

Ancient 0579
Medieval 0581
Modern 0582
Black 0328
African 0331
Asia, Australia and Oceania 0332
Canadian 0334
European 0335
Latin American 0336
Middle Eastern 0333
United States 0337
History of Science 0585
Law 0398
Political Science
    General 0615
    International Law and
        Relations 0616
    Public Administration 0617
Recreation 0814
Social Work 0452
Sociology
    General 0626
    Criminology and Penology ... 0627
    Demography 0938
    Ethnic and Racial Studies 0631
    Individual and Family
        Studies 0628
    Industrial and Labor
        Relations 0629
    Public and Social Welfare 0630
    Social Structure and
        Development 0700
    Theory and Methods 0344
Transportation 0709
Urban and Regional Planning 0999
Women's Studies 0453

THE SCIENCES AND ENGINEERING

BIOLOGICAL SCIENCES
Agriculture
    General 0473
    Agronomy 0285
    Animal Culture and
        Nutrition 0475
    Animal Pathology 0476
    Food Science and
        Technology 0359
    Forestry and Wildlife 0478
    Plant Culture 0479
    Plant Pathology 0480
    Plant Physiology 0817
    Range Management 0777
    Wood Technology 0746
Biology
    General 0306
    Anatomy 0287
    Biostatistics 0308
    Botany 0309
    Cell 0379
    Ecology 0329
    Entomology 0353
    Genetics 0369
    Limnology 0793
    Microbiology 0410
    Molecular 0307
    Neuroscience 0317
    Oceanography 0416
    Physiology 0433
    Radiation 0821
    Veterinary Science 0778
    Zoology 0472
Biophysics
    General 0786
    Medical 0760

EARTH SCIENCES
Biogeochemistry 0425
Geochemistry 0996

Geodesy 0370
Geology 0372
Geophysics 0373
Hydrology 0388
Mineralogy 0411
Paleobotany 0345
Paleoecology 0426
Paleontology 0418
Paleozoology 0985
Palynology 0427
Physical Geography 0368
Physical Oceanography 0415

HEALTH AND ENVIRONMENTAL SCIENCES
Environmental Sciences 0768
Health Sciences
    General 0566
    Audiology 0300
    Chemotherapy 0992
    Dentistry 0567
    Education 0350
    Hospital Management 0769
    Human Development 0758
    Immunology 0982
    Medicine and Surgery 0564
    Mental Health 0347
    Nursing 0569
    Nutrition 0570
    Obstetrics and Gynecology .. 0380
    Occupational Health and
        Therapy 0354
    Ophthalmology 0381
    Pathology 0571
    Pharmacology 0419
    Pharmacy 0572
    Physical Therapy 0382
    Public Health 0573
    Radiology 0574
    Recreation 0575

Speech Pathology 0460
Toxicology 0383
Home Economics 0386

PHYSICAL SCIENCES
Pure Sciences
Chemistry
    General 0485
    Agricultural 0749
    Analytical 0486
    Biochemistry 0487
    Inorganic 0488
    Nuclear 0738
    Organic 0490
    Pharmaceutical 0491
    Physical 0494
    Polymer 0495
    Radiation 0754
Mathematics 0405
Physics
    General 0605
    Acoustics 0986
    Astronomy and
        Astrophysics 0606
    Atmospheric Science 0608
    Atomic 0748
    Electronics and Electricity 0607
    Elementary Particles and
        High Energy 0798
    Fluid and Plasma 0759
    Molecular 0609
    Nuclear 0610
    Optics 0752
    Radiation 0756
    Solid State 0611
Statistics 0463

Applied Sciences
Applied Mechanics 0346
Computer Science 0984

Engineering
    General 0537
    Aerospace 0538
    Agricultural 0539
    Automotive 0540
    Biomedical 0541
    Chemical 0542
    Civil 0543
    Electronics and Electrical 0544
    Heat and Thermodynamics ... 0348
    Hydraulic 0545
    Industrial 0546
    Marine 0547
    Materials Science 0794
    Mechanical 0548
    Metallurgy 0743
    Mining 0551
    Nuclear 0552
    Packaging 0549
    Petroleum 0765
    Sanitary and Municipal 0554
    System Science 0790
Geotechnology 0428
Operations Research 0796
Plastics Technology 0795
Textile Technology 0994

PSYCHOLOGY
General 0621
Behavioral 0384
Clinical 0622
Developmental 0620
Experimental 0623
Industrial 0624
Personality 0625
Physiological 0989
Psychobiology 0349
Psychometrics 0632
Social 0451

♲

TURBULENT BURNING RATES OF

NEAR-FLAMMABILITY-LIMIT H_2-AIR-STREAM MIXTURES

BY

JANET V. LOESEL SITAR

A Thesis submitted to the Faculty of Graduate Studies of the University of Manitoba
in partial fulfillment of the requirements of the degree of

MASTER OF SCIENCE

© 1995

ABSTRACT

The effect of turbulence on the combustion of near-flammability-limit H_2-air-steam mixtures was examined in a 12 cm x 12 cm x 35 cm combustion chamber. The gas mixture was ignited by an electrical spark. Turbulence was generated by a perforated plate drawn across the combustion chamber. The perforated plate turbulence was characterized by hot-wire anemometry measurements made behind a perforated plate in a wind tunnel. The root mean square turbulent fluctuating velocity in the combustion chamber was varied by adjusting the plate velocity and the ignition delay relative to the movement of the plate. The instantaneous burning velocity was calculated from the pressure record measured inside the combustion chamber, assuming the flame to be spherical in shape. Laminar burning velocities of the mixture were measured in the same way. Experiments were performed using 6%-10% H_2-air mixtures with 0%, 10%, 20%, and 30% added steam. A relationship between the normalized turbulent burning velocity and the normalized fluctuating turbulent velocity was derived from these results, as well as critical turbulence levels. The results agree, qualitatively, with the work of Ballal and Lefebvre and of Abdel-Gayed, Bradley, and Lawes.

ACKNOWLEDGEMENTS

® Registered Trademark of Atomic Energy of Canada Limited.

Table of Contents

LIST OF FIGURES

LIST OF TABLES

vi

NOMENCLATURE

a,b - Coefficients in the equation of turbulence decay

D - Diameter of holes in the perforated plate

E1,E2 - Output voltages of the x-wire anemometer

K - Karlovitz stretch factor, $(0.157 \times (u'/S_L)^2 \times Re_L^{-0.5})$

L - Integral length scale of turbulence

Le - Lewis number (mass diffusivity/thermal diffusivity)

ΔP_c - Pressure drop across the wind tunnel contraction

Q - Flow velocity measured by the x-wire probe

R_F - Flame kernel radius

Re_L - Turbulent Reynolds number $(u'L/\upsilon)$

S_L - Laminar burning velocity

S_T - Turbulent burning velocity

$\tilde{u}$ - Instantaneous streamwise velocity in the wind tunnel

$\tilde{v}$ - Instantaneous transverse velocity in the wind tunnel

u - Instantaneous streamwise fluctuating velocity in the wind tunnel

v - Instantaneous transverse fluctuating velocity in the wind tunnel

u' - r.m.s. fluctuating turbulent velocity in the streamwise direction

v' - r.m.s. fluctuating turbulent velocity in the transverse direction

$\overline{U}$ - Average streamwise fluid velocity in the wind tunnel

$\overline{U}_i$ - Average fluid velocity in the wind tunnel at axial location i.

$\overline{U}_{ref}$ - Average fluid velocity in the wind tunnel at reference location x/D=20

V_p - Velocity of the perforated plate in the combustion chamber

x/D - Distance behind the perforated plate in the wind tunnel, non-dimensionalized by the hole diameter

x/b - Distance behind a grid in the wind tunnel, non-dimensionalized by the grid bar size.

δ_L - Laminar flame thickness

γ - Pitch angle of the x-wire probe during calibration

η - Kolmogorov microscale

υ - Kinematic viscosity

1.0 INTRODUCTION

In certain postulated loss-of-coolant accidents, hydrogen gas can be released into the containment buildings from zirconium-steam reactions in the reactor core. If the hydrogen mixes with air and is ignited, the resulting combustion pressure could pose a threat to the containment structures and other essential equipment. The effect of combustion on the pressure rise inside the containment building will depend on the burning rate of the combustible mixture, which is strongly affected by turbulence initially present or caused by obstacles in the flame path. The hydrogen and steam produced in a severe accident will mix with the large volume of air in the containment building. In CANDU reactors where igniters are used to burn off the hydrogen as it builds up, only near-flammability-limit mixtures would be seen in the containment. An understanding of the combustion of these mixtures at different turbulence levels is needed to better define the safety margin of nuclear reactors under accident conditions.

Freely expanding flames are intrinsically unstable. The flame shape and the reaction rate in the reaction zone are easily influenced by the local flow field. Turbulence generated by fans or by combustion-induced flow-obstacle interaction can cause the local burning rate to increase as a result of flame folding and high mass transport in the turbulent flow field. However, excessive flame stretching and rapid mixing in a turbulent flow field can significantly lower the flame temperature and cause local quenching. Available empirical expressions that relate the burning rate to the turbulence parameters (also known as flame laws), are based mainly on experimental data from near-stoichiometric fuel-oxidant mixtures. Moreover, these flame laws account only for the positive aspects of turbulence and thus cannot fully quantify the effects of turbulence on combustion. As a result, models using available flame laws predict that all flames can accelerate continuously to detonation velocities. It is well known that in an insensitive mixture such as a near-flammability-limit H_2-air-steam mixture, a flame cannot accelerate indefinitely to detonation velocity. There exists a

maximum flame speed (a steady state velocity) associated with a given set of initial and boundary conditions. This maximum value is a result of the competition between the positive and the negative aspects of turbulence on combustion. If a flame can be quenched readily by turbulence, the maximum flame speed is relatively low (less than one hundred meters per second). Transition to detonation in this mixture is therefore very unlikely and the associated overpressures are bounded by the adiabatic constant volume combustion pressure.

The aim of this thesis is to better understand and quantify the interactions of two complex phenomena: turbulence and combustion. Previous studies have approached this problem in two ways: analytically and experimentally. Because of the complexity of the turbulent fluid dynamics, analytical solutions need to involve assumptions and simplified models. Experimental work is generally carried out to check the validity of analytical models and to gain insight into the physical processes. The present work falls into the latter category. The next section will discuss the work of some other combustion researchers and how it relates to the present problem. This will be followed by an outline of the thesis.

1.1 LITERATURE REVIEW

Ballal and Lefebvre[9] have studied the structure and propagation of turbulent flames using a rectangular combustion chamber with turbulence controlled by a grid located upstream of the combustion zone. They examined the burning of propane-air mixtures in different turbulent environments by using various grids to create different values of turbulence intensity, length scale, and vorticity. Three distinct burning regimes were identified, as shown in Figure 1.1, each having a distinct relationship between turbulence and burning velocity. In regime 1, where turbulence levels are low, flame wrinkling is caused by eddies larger than the laminar flame thickness, δ_L. Wrinkling increases the flame surface area and hence the mass burning rate. Turbulent flame

speeds in regime 1 depend on the parameter $u'L/(S_L\delta_L)$. (In this parameter, u' is the r.m.s. fluctuating velocity of the cold unburnt mixture behind the plate, L is the turbulent integral length scale, and S_L is the laminar burning velocity). In regime 2, eddies that are both larger and smaller than the laminar flame thickness affect the structure of the flame. The flame surface is highly wrinkled and broken, with pockets of fresh mixture entrained in the reaction zone. Ballal and Lefebvre observed that the burning velocity in this regime was approximately equal to twice the laminar flame speed. Regime 3 contains strong turbulence in which most of the eddies are smaller than the laminar flame thickness, causing high burning rates and a thick reaction zone. In this regime, the turbulent burning velocity depends on $u'\delta_L/(S_L\eta)$. (η is the Kolmogorov microscale). Only burning regime 3 is relevant to the results discussed in this paper, and these results will be compared to Ballal and Lefebvre's relationship for this regime.

Al-Khishali, Bradley and Hall[5] have studied the turbulent combustion of near-limit H_2-air mixtures with turbulence produced by four fans in a combustion bomb. The flame structure was determined from schlieren photographs. These photographs showed that the sideways and downward flame propagation speeds first increased, then decreased with increasing turbulence for mixtures of 5-10% H_2-air (where 5% H_2-air means 5% H_2 by volume and 95% air by volume). The pressure rise showed the same trend for mixtures of 5-8% H_2-air. For more sensitive mixtures, the pressure rise only increased with increasing turbulence intensity, for the range tested. This work provided some useful information on the effects of turbulence on near-flammability-limit mixtures, although no attempt was made to measure an overall turbulent burning velocity or use the results to formulate a flame law.

Abdel-Gayed et al.[1,2,3,4] have developed theories and experimental correlations of the relationship between turbulent parameters and burning velocity. They have reviewed data from many studies, including their own, and presented these data in terms of the normalized turbulent burning velocities, S_T/S_L, the normalized r.m.s.

3

turbulent velocities, u'/S_L, and the turbulent Reynolds number, Re_L. (S_T is the turbulent burning velocity, or speed of the flame relative to the unburnt gas, and $Re_L = u'L/\nu$, where ν is the kinematic viscosity of the unburnt gas). Abdel-Gayed and Bradley started with the Two-Eddy Theory of Premixed Combustion[1], which simplifies the spectrum of turbulence into two principal eddy sizes. By postulating that burning within the eddies is essentially a molecular phenomenon, they could couple the eddy decay rate with the amount of chemical reaction during an eddy lifetime. This model was later refined[2] to allow for flame straining reductions in laminar burning velocity, as applied to turbulent burning. Further refinements[3] to the model include using additional dimensionless parameters for the correlation of the experimental results. The new parameters are the Karlovitz stretch factor, K, which is the ratio of chemical to eddy lifetimes and defined by Abdel-Gayed et al. as $K=0.157 \times (u'/S_L)^2 \times Re_L^{-0.5}$, the Lewis number, Le, which is the ratio of mass diffusivity to thermal diffusivity, and a new parameter, called the effective r.m.s. turbulent velocity. A flame developing from a point source is not immediately affected by the full spectrum of turbulence, and this is taken into account by using an effective r.m.s. turbulent velocity. Abdel-Gayed, Bradley and Lung[4] later defined different burning regimes using the collated results from [1]. These regimes are described as (1) the continuous laminar flame sheet, (2) the break-up of the continuous flame sheet, (3) the development of quenching in a fragmented reaction zone, and (4) flame quenching. These regimes are defined in terms of K, the Karlovitz stretch factor, and Le, the Lewis number. Abdel-Gayed et al. claimed that these regions can tentatively predict flame quenching. Further work on the correlation of turbulent burning velocities in terms of K×Le as well as in terms of flame extinction stretch rates was done by Bradley, Lau, and Lawes[12]. This ongoing work at Leeds University is important because the group uses experimental data from many fuels, mixtures strengths, and apparatus to verify and strengthen the generality of their correlations and analytical theories. There is, however, an appreciable scatter in the data used for the dimensionless groups. Because of this scatter, and because of the lack of data at near-flammability-limit mixtures, these correlations should not be used without the

4

verification of further experiments to see if near-flammability-limit H_2-air-steam mixtures follow the same trends.

Checkel et al. [13,14,15,16,26] have investigated the turbulent burning of propane-air and methane-air mixtures in a cubical combustion chamber in which turbulence was generated by the movement of a perforated plate. The flame was initiated by a spark in the centre of the chamber. The turbulent fluctuating velocity generated in this apparatus was determined by making hot-wire anemometry measurements in both the combustion chamber and behind the perforated plate in a wind tunnel. Assuming that the flame kernel was a thin-shelled sphere, Checkel calculated the burning velocity from the rate of pressure rise in the combustion chamber. Checkel and Thomas[14] studied the effect of the rate of strain on the burning rate of propane-air mixtures. They estimated the rate of strain by using dissipation rates derived from anemometry measurements. The decay of turbulence during combustion and the effect of compression on both burning velocity and turbulence were taken into account. Their results reinforced the idea that turbulence has both an enhancing effect and a quenching effect on burning velocity.

1.2   OBJECTIVES AND OUTLINE OF PRESENT STUDY

The present study is an extension of Checkel's investigation. This thesis presents experimental results of the turbulent burning velocities for near-flammability-limit H_2-air-steam mixtures. An apparatus similar to that of Checkel[13] was used to produce pressure-time histories of turbulent burns, which were converted to burning velocities. By assuming that the flame kernel is thin-shelled and spherical, a flame speed relative to the unburned gas, referred to as the turbulent burning velocity, S_T, can be calculated. Turbulence levels are based on hot-wire measurements made behind a perforated plate in a wind tunnel. From the results, a relationship between turbulence

and combustion is developed (S_T/S_L vs. u'/S_L). Critical turbulence levels, defined as the level of turbulence beyond which no burning is possible in the apparatus due to quenching, are determined for several mixtures. The results are compared to the correlations of Abdel-Gayed, Bradley and Lung[4] and of Ballal and Lefebvre[9].
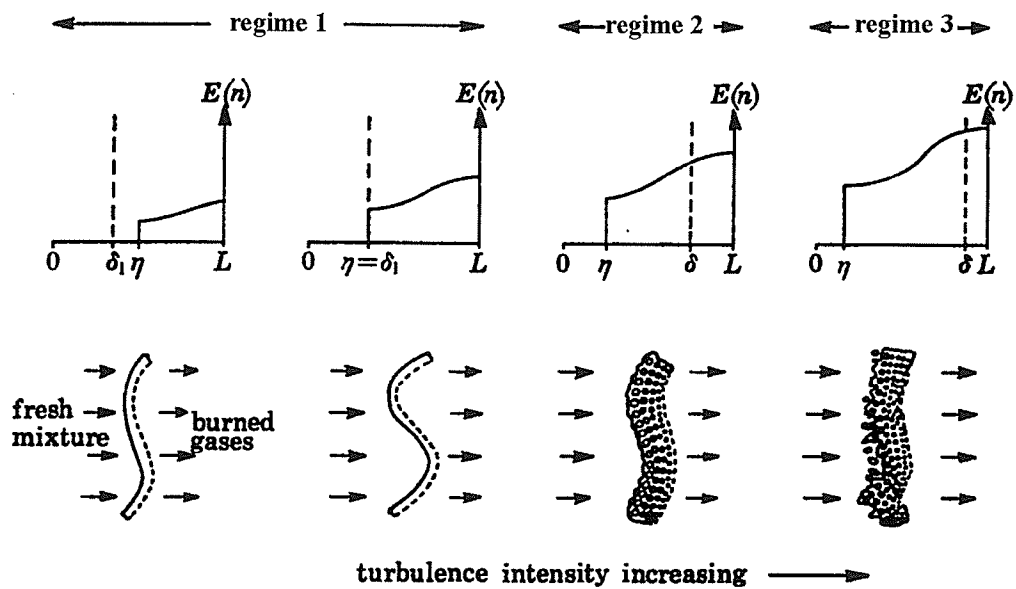
Figure 1.1: Diagrams illustrating the effect of different levels of turbulence on flame structure. Taken from Ballal and Lefebvre[9].

NOTE: E(n) is the turbulence kinetic energy and is plotted against the turbulence length scale.

2.0 EXPERIMENTAL SET-UP AND PROCEDURE

Turbulence was produced in a 12 cm × 12 cm × 35 cm combustion chamber by traversing a perforated plate across the chamber. A schematic of the system is shown in Figure 2.1. The momentum of a drop-weight was transferred to the plate using a pulley and rope system. The plate speed was determined directly from the output of an optical sensor attached to the plate driver assembly. Plate velocities of up to 10 m/s were achieved. A perforated plate with 20 mm diameter holes (60% blockage ratio) was used to produce turbulence, shown in Figure 2.2.

The hydrogen and air were delivered in the desired proportions by two Brooks 5850 electronic flowmeters. The steam flow rate was controlled by using a calibrated pump to deliver water to the steam generator. Mixture compositions were periodically verified by a Nova thermal conductivity hydrogen meter. Pressure in the combustion chamber was measured by a PCB (model 113A24) piezoelectric transducer located in the combustion chamber wall and recorded by a digital oscilloscope (Tektronics 2224). The pressure trace was then transferred to a computer (using a GPIB data acquisition board) for further analysis.

An electronic timing system was used to control the igniter and to trigger the camera shutter relative to the plate movement. The igniter extends to the centre of the chamber and provided a 30 kV spark. Two parallel windows located on opposite sides of the chamber allowed direct observation of the flame using conventional schlieren technique. A xenon arc lamp was used as a light source. High speed schlieren photographs (1500 frames/second) were taken using a Beckman and Whitley Model 351 Drum Streak camera.

The combustion experiment began by flushing the combustion chamber with at least five volumes of H_2-air-steam to ensure that the desired mixture was achieved. The drop weight was then positioned at the proper height on the guide post and dropped.

8

When the weight passed an optical sensor, the electronic delay system controlled the remaining events: ignition, acquisition of the data on an oscilloscope, and triggering of the camera. After transferring the digitized signal from the oscilloscope to the computer, a polynomial equation was fitted to the pressure-time curve and the burning velocity was calculated.
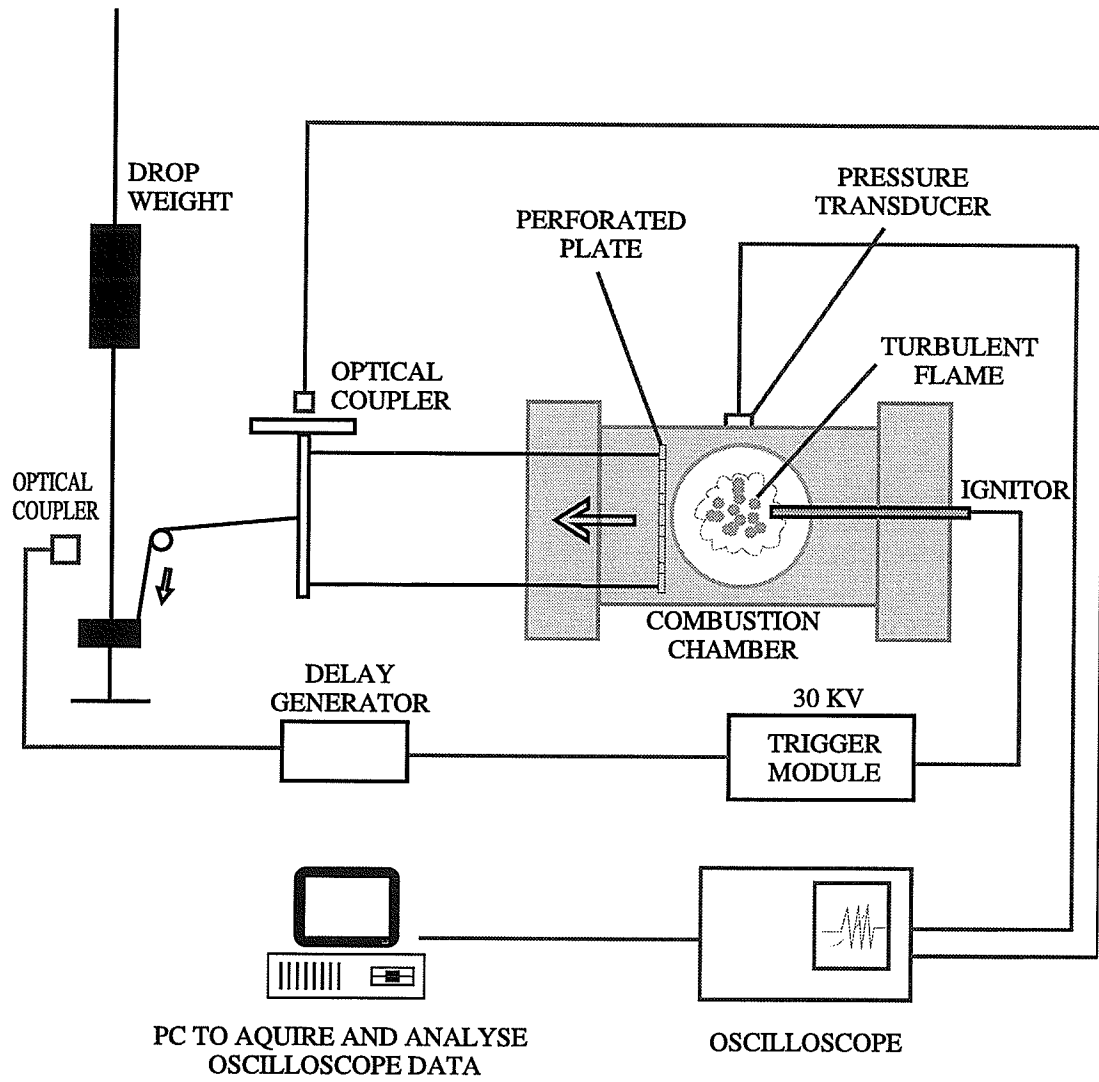
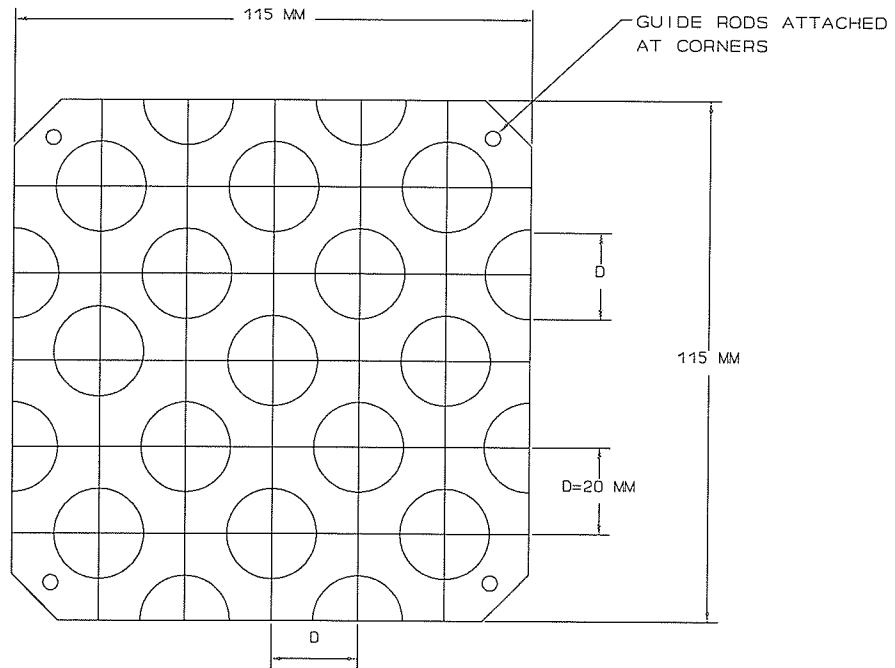**Figure 2.1:** Schematic of the combustion chamber and the turbulence generating apparatus.

Figure 2.2:   Schematic of the 20 mm hole diameter plate.

3.0 TURBULENCE ANALYSIS

The decay of turbulence in time at a stationary location behind the moving perforated plate is basically the same as the decay of turbulence with increasing distance behind the perforated plate in a wind tunnel. The only difference in the flows is that in a wind tunnel, there is a mean velocity superimposed on the turbulence. It is generally accepted that in a constant-area wind tunnel test section, the mean velocity does not affect the decay of the turbulence intensity. For example, far downstream of the plate, data plotted in terms of the ratio of r.m.s. fluctuating velocity to mean velocity versus non-dimensionalized distance from the plate collapses onto one line in the results of Baines and Peterson[8]. Measuring turbulent velocities with a hot-wire anemometer is much easier in the wind tunnel than in the combustion chamber for two reasons. Firstly, turbulence created by a moving plate has a negligible mean velocity, causing the turbulence intensities to be high and the hot-wire measurements to be inaccurate. Secondly, the turbulence is transient, requiring an ensemble average of data from numerous trials to produce statistically meaningful results. A laser doppler anemometer with frequency switching would not be hampered by these constraints, but unfortunately, the equipment is not available at the University of Manitoba. Therefore, turbulence parameters for this work were measured in a wind tunnel using a hot-wire anemometer.

Many researchers have studied the decay of turbulence far downstream of grids and perforated plates including Baines and Peterson[8], Comte-Bellot and Corrsin[17], and Uberoi and Wallace[30]. This report concentrates on the highly turbulent region immediately behind the plate. The turbulence in this region has also been studied by Checkel[13] and McDonell[26] using hot-wire anemometry measurements behind a perforated plate in a wind tunnel, and behind a moving perforated plate in a combustion chamber. Checkel found good agreement between the anemometer output produced by the movement of the perforated plate in the combustion chamber and the r.m.s. fluctuating velocity produced in the wind tunnel by using a Gaussian statistical

model of non-isotropic turbulence to relate the two results. The present work assumes that turbulent characteristics behind a plate in a wind tunnel corresponds directly to turbulence characteristics behind a moving plate. Measurements were made behind three plates with different hole diameters, although only one plate (with 20 mm diameter holes) was used in the combustion experiments. These plates will be referred to as the 20 mm plate (20 mm diameter holes), the 10 mm plate (10 mm diameter holes), and the 5 mm plate (5 mm diameter holes). Details of the experimental set-up, calibration, and uncertainty analysis of the hot-wire anemometry measurements are described in Appendix A.

Figure 3.1 shows the measured streamwise turbulence intensity and the exponential curves used to describe the turbulence decay. Error bars indicate the range of experimental uncertainty. To optimize the fit, two curves are used for each plate, one for data between $5<x/D<15$ and one for $15<x/D<60$. An overall fit for all the plates is also calculated by taking the arithmetic average of the coefficients for each data range. The coefficients, as well as the chi^2 value and standard error (SE), are listed in Table 1, for the equation

$$\frac{u'}{U} = a*\left(\frac{x}{D}\right)^b \qquad (1)$$

Figure 3.2 compares the streamwise turbulence intensities to lattice-type grid-generated turbulence intensity data measured by Baines and Peterson[8] and to fitted equations for perforated plate turbulence intensities measured by McDonell[26]. McDonell's measurements are essentially a refinement of Checkel's[13] work. The turbulence intensities were presented in terms of x/b, the distance downstream of the plate non-dimensionalized by the lattice bar size. The equivalent bar size for a perforated plate was calculated by assuming a lattice of equal wetted perimeter and fraction open area, so that

13

$$b = D*\left(\sqrt{\frac{8}{\pi}} - 1\right) \qquad (2)$$

Table 1:   **Equation coefficients for the decay of turbulence intensity downstream of the perforated plates in the wind tunnel.**

Plate	a	b	χ^2	SE(a)	SE(b)
20 mm: 5≤x/D≤15	4.295	-1.405	0.0012	2.658	0.3135
15≤x/D≤60	0.5205	-.6346	0.0000114	0.1353	0.08689
10 mm: 5≤x/D≤15	3.596	-1.347	0.00021	0.6195	0.09516
15≤x/D≤60	0.4714	-0.5916	0.0000131	0.09074	0.06153
5 mm: 5≤x/D≤15	4.769	-1.523	0.00014	0.7464	0.08765
15≤x/D≤60	0.5547	-0.721	0.0000041	0.058	0.03244
Average:5≤x/D≤15	4.220	-1.425	-	-	-
15≤x/D≤60	0.5515	-0.649	-	-	-

The turbulence intensities agree best with Baines and Peterson in the region where turbulent flow has become well established, i.e. x/b>10, which corresponds to x/D>6.

The decay rates for the three plates calculated from 15<x/D<60 agree fairly well with the one used by Baines and Peterson, in the equation

$$\frac{u'}{\overline{U}} = 1.12 * \left(\frac{x}{b}\right)^{-\frac{5}{7}} \tag{3}$$

The decay exponents for the 20 mm, 10 mm, and 5 mm plates, for 15<x/D<60, are -0.6346, -0.5916, and -0.721, respectively. These exponents are 11% lower, 17% lower, and 1% lower, respectively, than (-5/7), while the averaged fit is -0.649, which is 9% lower than (-5/7). This is reasonably good agreement considering that the equations were fitted to data measured over shorter downstream distances than Baines and Peterson's data, and produced by turbulence behind perforated plates, not grids. Decay rate exponents calculated for grid-generated turbulence by Comte-Bellot and Corrsin[17] vary from 0.72-0.85, while those calculated by Uberoi and Wallace[30] are between 0.7-0.8. McDonell's[26] exponents are slightly higher, between 0.8-0.9, probably because his equation was fitted to data from 10<x/D<40, a rather short range in the high turbulence region.

The turbulence intensity values agree fairly well with McDonell's work. Agreement is within the experimental uncertainty of this work between 10<x/D<30 for the 20 mm and 10 mm plates, and between 30<x/D<60 for the 5 mm plate. The 5 mm plate has a similar decay rate but lower (~15%) turbulence intensities for x/D<30 than McDonell's work. The 10 mm plate has slightly higher values compared to McDonell in the region farthest from the plate, x/D>30.

The turbulence intensity values measured close to the plates, from 5<x/D<15, may be less accurate than those measured farther from the plate, due to the inherent inaccuracy of hot-wire response in highly turbulent inhomogeneous flow.

In the combustion chamber, the turbulence intensity affecting the flame is determined

15

by using equation 1, with the 20 mm plate coefficients from Table 1. The parameter x/D becomes $(V_p \times t)/D$, where V_p is the plate speed, D is the plate hole diameter, and t is the time between the plate passing the igniter and the flame kernel radius reaching 3 cm. Similarly, in $u'/\overline{U}$, $\overline{U}$ is replaced by V_p. To allow comparisons of the combustion work to other researchers, McDonell's[26] equations for integral length scale and Kolmogorov microscale are also used to characterize the turbulence. These are also exponential in form, and the coefficients are listed in Table 2.

$$\frac{SCALE}{D} = a * \left(\frac{x}{D}\right)^b \tag{4}$$

Table 2: **Equation coefficients for the decay of turbulence length scale behind the perforated plate, taken from McDonell[26].**

Scale	a	b
Integral	0.13	0.4
Kolmogorov	0.001	0.786
Taylor	0.034	0.465

It is assumed that although the measured turbulence intensities for the present work and McDonell's work are not exactly the same, they are close enough that McDonell's values for length scales are reasonable estimates of the length scales in our apparatus. All turbulence intensities will be calculated from the results of this work, and all length scales will be calculated using McDonell's equations.
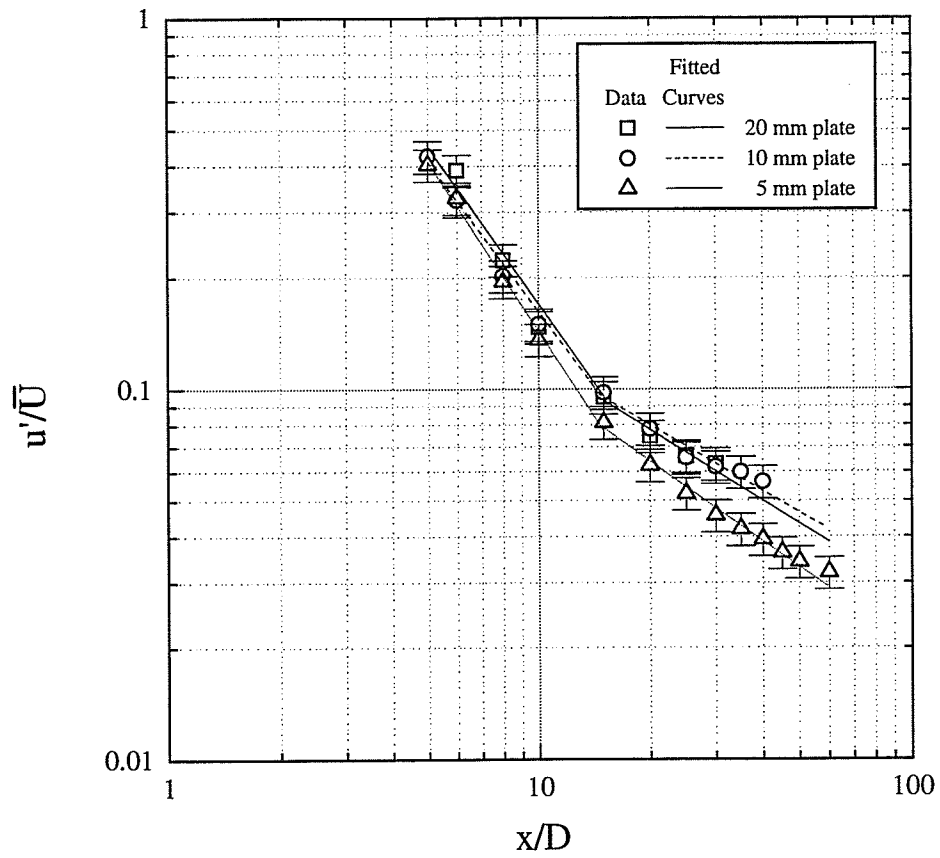
Figure 3.1 Experimental turbulence intensities for each plate and their corresponding fitted equations.
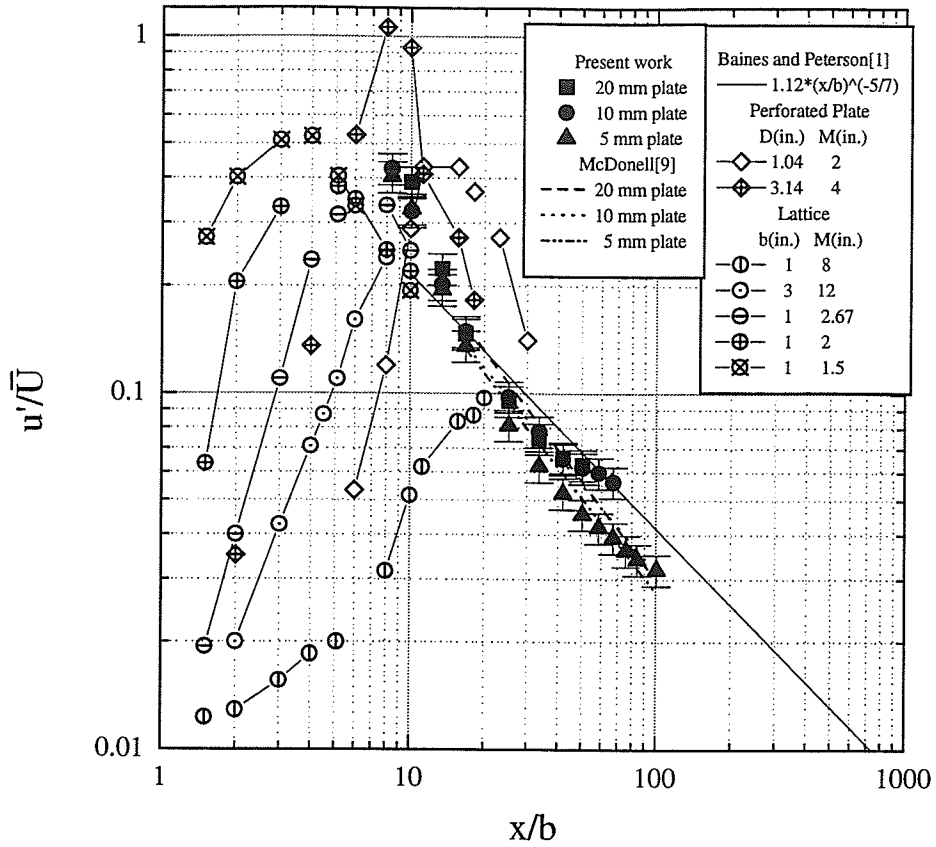
Figure 3.2   Comparison of measured turbulence intensities to lattice-generated turbulence data from Baines and Peterson[8] and to fitted equations of perforated plate data from McDonell[26].

4.0   BURNING VELOCITY ANALYSIS

Burning velocity is defined as "the relative velocity, normal to the flame front, with which the unburnt gas moves into this front and is transformed" (Rallis and Garforth[28]). The laminar burning velocity is considered to be an intrinsic property of a specific combustible mixture. Turbulent burning velocities are strongly affected by the r.m.s. fluctuating velocity of the turbulence and possibly by other turbulence characteristics such as length scale. Turbulence can have both an enhancing and quenching effect on burning velocity. Various methods have been used over the years to determine burning velocities. They include the bunsen burner, soap bubble, cylindrical tube, and double kernel methods. The method used in this paper uses the pressure-time history of a spherical flame kernel in a constant volume vessel.

Burning velocities of near-flammability-limit laminar flames are difficult to define or measure. These flames are very unstable, being affected by both buoyancy and by selective diffusional demixing, and tend to become mushroom-shaped as they burn. Burning velocities of very turbulent flames are also difficult to define since the flames do not usually resemble a thin-shelled expanding flame kernel, but rather a thick brush of burning eddies. A method has been proposed for calculating the burning velocities for small expanding flame kernels using only the pressure record of the burn. (See Appendix B for the derivation). This "pressure trace" method assumes that the flame kernel is spherical in shape, and that the pressure rise is very small. It also assumes that the pressure rise caused by combustion in a constant volume is proportional to the volume of gas already burned. Burning velocities can be calculated for both laminar and turbulent flames. Since the thin-shelled spherical flame assumption is only a convenient construction and not an accurate description of reality, the calculated burning velocities should be considered as averaged or effective burning velocities. A polynomial is fitted to the pressure-time history of the burn and the derivative of this curve is used to calculate the burning velocity. Precompression of the unburnt gas does not become significant until the flame kernel is very close to the wall and is

therefore ignored. The pressure trace method is a particular case of the more generalized burning velocity equations developed by Rallis et al.[28]. Rallis's equations use values of the flame radius as a function of time, and therefore require schlieren photographs of the flame expansion. When burning velocities calculated using both methods are compared, they agree to within 20% for 6-10% H_2-air mixtures, and to within 10% for richer mixtures. This is marginal agreement, but significant error is introduced in the estimation of the flame radius from the schlieren photographs, and in the assumption of a spherical flame in the pressure trace method, when the flame kernel is not spherical. Rallis and Garforth have developed a thick flame equation that might be more accurate for near-flammability-limit laminar flames, or highly turbulent flames, but the author is not aware of any data available on typical laminar flame thicknesses for the mixtures studied, so this method could not be tested. In this thesis, the pressure trace method for calculating the burning velocity is presented because it is more convenient to use than Rallis and Garforth's method, which requires analysis of schlieren photographs for each burn.

A freely expanding flame kernel in a constant volume combustion vessel can grow quite large before there is a significant pressure rise in the vessel. Once the flame kernel touches the wall, the pressure record can no longer be used to calculate burning velocity because the pressure is affected by heat loss to the wall. As a result, only the burning velocity of a flame kernel which has a diameter smaller than the width of the combustion chamber can be used for this analysis. This flame has a maximum radius of about 6 cm for the turbulent flames and 3-4 cm for the buoyant laminar flames. The current analysis uses data from flames with radii of 3 cm for the turbulent flames and 2 cm for the laminar flames. The laminar flame radius is limited to 2 cm because buoyancy causes the leanest flames to float up and touch the combustion chamber roof before the flame kernel has grown very large.

The results of the laminar burning velocity measurements for H_2-air-steam mixtures are plotted in Figure 4.1. A visual best fit curve was drawn through these results to

define the laminar burning velocities. Some results for dry laminar burning velocities measured by Koroll[23] using the double kernel method are presented for comparison. In general, the pressure trace method gives a slightly lower value of burning velocity.

A typical pressure record for a laminar 6% H_2-air burn is shown in Figure 4.2. The laminar burning velocities were calculated using the marked portion of the pressure curve. Schlieren photographs show that the dip in the pressure curve corresponds to the flame kernel touching the top wall of the combustion chamber. The pressure rise at this portion of the curve corresponds to 0-1.5% of the adiabatic constant volume combustion rise, and 0-2.4 kPa. Most of the fuel in the combustion chamber remained unburned, as is typical for extremely lean mixtures.
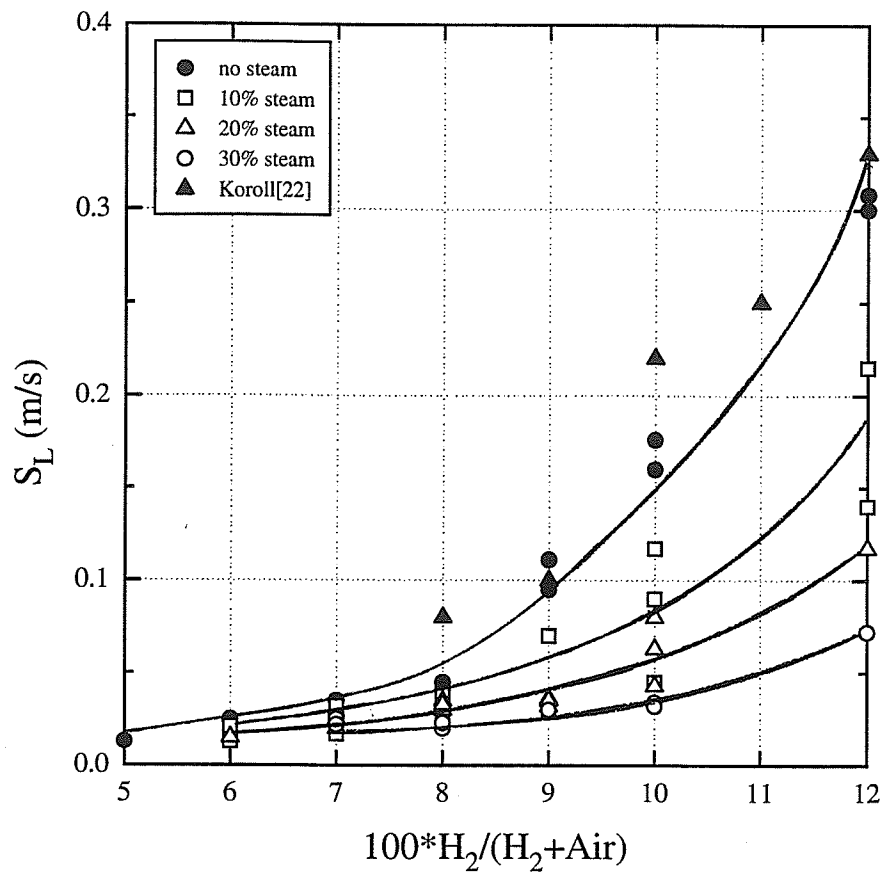
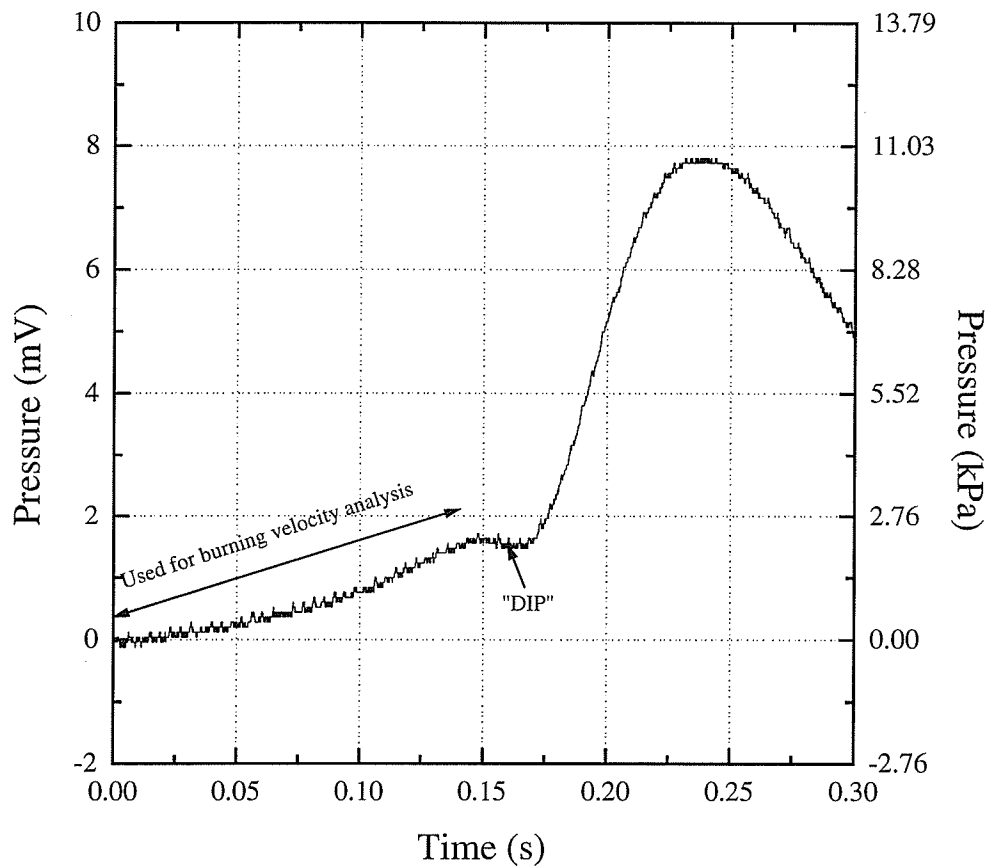**Figure 4.1:** Laminar burning velocities for lean hydrogen-air-steam mixtures.

Figure 4.2: Pressure record for a 6% H_2-air laminar burn.

5.0   RESULTS AND DISCUSSION

The test conditions were chosen to examine the effects of various turbulence levels on a range of near-flammability-limit H_2-air-steam mixtures. Mixture compositions tested were 6%-10% H_2 in air and 6-10% H_2 in air plus 10%, 20%, and 30% steam. Normalized turbulent fluctuating velocities, u'/S_L, varied from 1 to 80. Schlieren photographs of the turbulent flame were useful in revealing flame structure and the burning process. For instance, Figure 5.1 shows a laminar 7% H_2-air flame. Since 7% H_2-air is below the downward propagation limit, buoyancy effects cause the flame to be distorted. The wrinkles on the flame surface are caused by the intrinsic instability of the flame itself. Figure 5.2 shows a flame of the same mixture, in a turbulent environment. The surface is corrugated, but the shape is still essentially spherical. Due to an increase in the surface area and mass transport, the overall burning rate is higher than that in the previous laminar case.

Figure 5.3 shows the results for all mixtures in one graph, with example error bars shown. Typical sources of uncertainty in the experiment include the mixture composition, which is accurate to about ±1.0% H_2, and the calculation of the burning velocity based on an 8th-order polynomial fitted to the pressure-time curve. The former contributes the most to the experimental uncertainty, which averages ±23%. The uncertainty in the measurement of the turbulence intensity is ±10%.

The data in Figure 5.3 show that the slope of the correlation for S_T/S_L versus u'/S_L approaches one. This implies that a simple flame law (e.g., $S_T/S_L = 1+u'/S_L$) can describe the effect of turbulence on burning rate fairly well. This is the most often used flame law, also known as the wrinkled flame model[7]. This flame law describes the results for sensitive fuel mixtures fairly well. Figures 5.4-5.7 show the data for each steam concentration. Examining the data in these figures shows that the wrinkled flame law can also be used to describe highly turbulent combustion of near-flammability-limit mixtures. At turbulence levels above u'/S_L=40, however, the data

24

seems to curve away from the wrinkled flame equation. This trend has also been observed by other researchers including Abdel-Gayed et al.[1] and Al-Khishali et al.[5], and occurs when the quenching effect of turbulence begins to equal the enhancing effect. However, in this apparatus there is an increased uncertainty in the measurements at high turbulence intensities, which could account for some or all of this trend.

The data also show critical turbulence levels for some mixture compositions beyond which total quenching of the flame occurs. These critical turbulence levels are shown on Figures 5.4-5.7 as vertical "walls". For example, no burning was achieved in dry mixtures, for u'/S_L exceeding 30 for 6% H_2. No burning was achieved in mixtures containing 10% steam, for u'/S_L exceeding 31 for 6% H_2, or u'/S_L exceeding 74 for 7% H_2. Similarly, the critical normalized turbulence levels for 7% and 8% H_2 (with 20% steam) were 36 and 55, respectively. With 30% steam, the critical normalized turbulence levels for 8% and 9% H_2 were 29 and 31, respectively. Presently, the apparatus does not create high enough turbulence levels to reach the critical levels for more sensitive mixtures.

Results in Figures 5.3-5.7 show a high degree of scatter. This scatter is not due mainly to experimental errors, but to the inherent irreproducibility of turbulence and turbulent burning. It is not possible to completely characterize a turbulent flow, and thus differences in the turbulent flow structure will cause differences in turbulent burning rate. As well, near the quenching limit, combustion becomes more susceptible to the effects of turbulence, since the turbulence time scales approach the chemical time scales. Near the quenching limit, flame stretching that causes an overall increase in the burning rate can also cause local quenching. This local quenching causes hot burned gases to mix with unburned gases. When this sensitive region reignites, the overall burning rate can be much higher than the original mixture. Thus it is reasonable to expect that a relatively small difference in turbulence intensity, causing local quenching in one flame but not in another, might cause a large difference in

burning velocity. The quenching and reignition process is not reproducible. Another possible contributing factor to the scatter is the variation in turbulence length scale sizes. Integral length scales in the experiment vary between approximately 7 mm and 14 mm, based on equations from McDonell[26], and different sizes of length scales are known to have different effects on combustion.

By calculating the Lewis number, Le, and the Karlovitz stretch factor, K (as defined in [3]), it is possible to characterize the present results in terms of the regimes suggested by Abdel-Gayed et al.[4]. The low turbulence data (from approximately $2 < u'/S_L < 10$) fall into the "continuous laminar flame sheet" regime and the "breakup of continuous flame sheet" regime, respectively. The higher turbulence data falls into the "development of quenching in fragmented reaction zone" regime. Only a very few of the data fall into the "flame quenching" regime. These points are the ones farthest below the wrinkled flame law line. Figure 5.8 compares the curves fitted through constant Reynolds number for the present data to Abdel-Gayed et al's. correlations. Similarly shaped curves are seen. However, the present data produce much higher turbulent to laminar burning rate ratios compared to Abdel-Gayed et al. at a given Reynolds number. There are a number of possibilities to account for these differences. Decaying turbulence in the present apparatus might affect combustion differently than the constant turbulence data that Abdel-Gayed et al. used to fit their curves. Turbulent burning mechanisms of near-flammability-limit mixtures are different than those of near-stoichiometric mixtures: lean turbulent flames are much more easily broken up than near-stoichiometric flames, which tend to remain as wrinkled flames. As a result, the burning rate of lean fuel-air mixtures is more affected by turbulence than that of near-stoichiometric fuel-air mixtures. Abdel-Gayed et al. used results mainly from near-stoichiometric fuel-oxidant mixtures. Therefore, although the present work gives results that do not quantitatively agree with Abdel-Gayed et al., experimental and physical differences are the likely causes.

The present experimental results have been classified into the three regimes of flame

structure as suggested by Ballal and Lefebvre[9]. The Kolmogorov scale was calculated using the experimental correlation of McDonell[26], and the laminar flame thickness was estimated as

$$\delta_L = \frac{v}{S_L}$$

from Gaydon and Wolfhard[19]. The kinematic viscosity, v, was calculated (at the unburnt gas temperature) by using Watson's data [31] for the viscosity of the component gases and calculating the viscosity of the mixed gases with Wilke's equation [32]. Incropera and DeWitt[21] was the source for the density values. The laminar flame speeds were experimentally determined using the same apparatus. It was determined that most of the data are in regime 3, where $\eta < \delta_L$ and $u' > 2S_L$. Figures 5.9 and 5.10 compare the present results with Ballal and Lefebvre's relation for regime 3, which is

$$\frac{S_T}{S_L} = 0.5 * \frac{u'\delta_L}{S_L\eta}$$

It can be seen that the present results fall along this line, with a lot of scatter, until $(0.5u'\delta_L)/(S_L\eta) = 50$. At higher values of this parameter, the data fall well below the line. Ballal and Lefebvre's work only included data for $(0.5u'\delta_L)/(S_L\eta) < 12$. These results suggest that their relation is inadequate to describe burning at the very high turbulence levels experienced in the present apparatus.
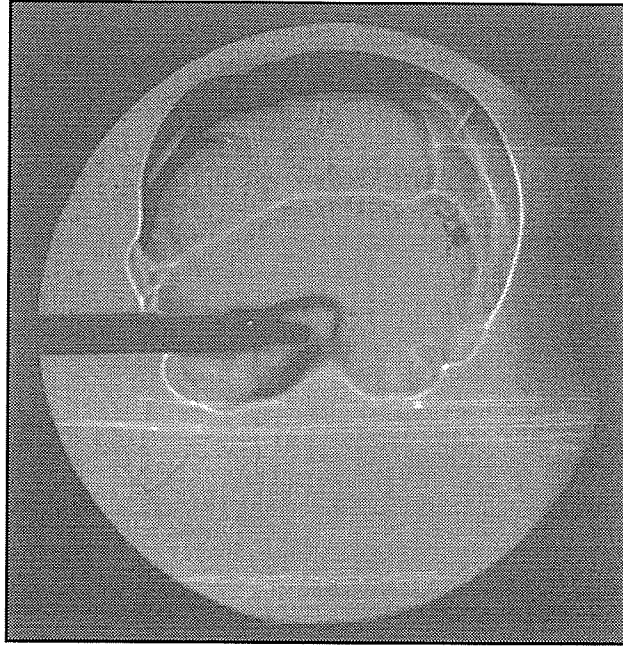
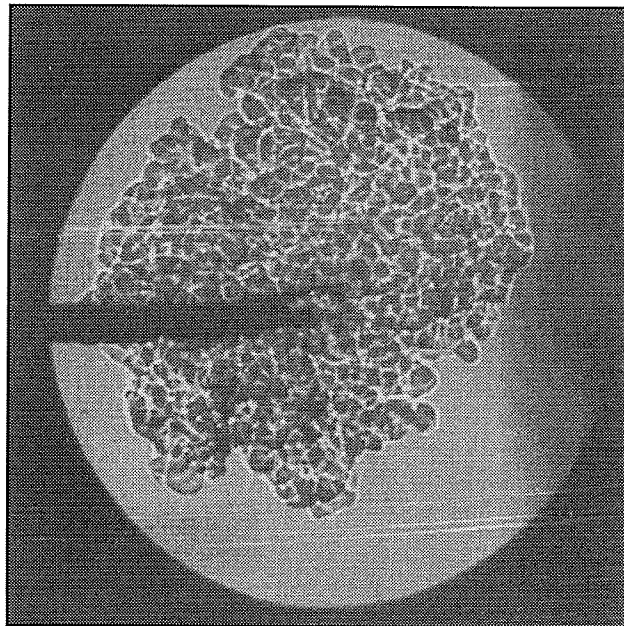**Figure 5.1:**   **Schlieren photograph of a laminar flame kernel.**

Figure 5.2:   **Schlieren photograph of a turbulent flame kernel.**
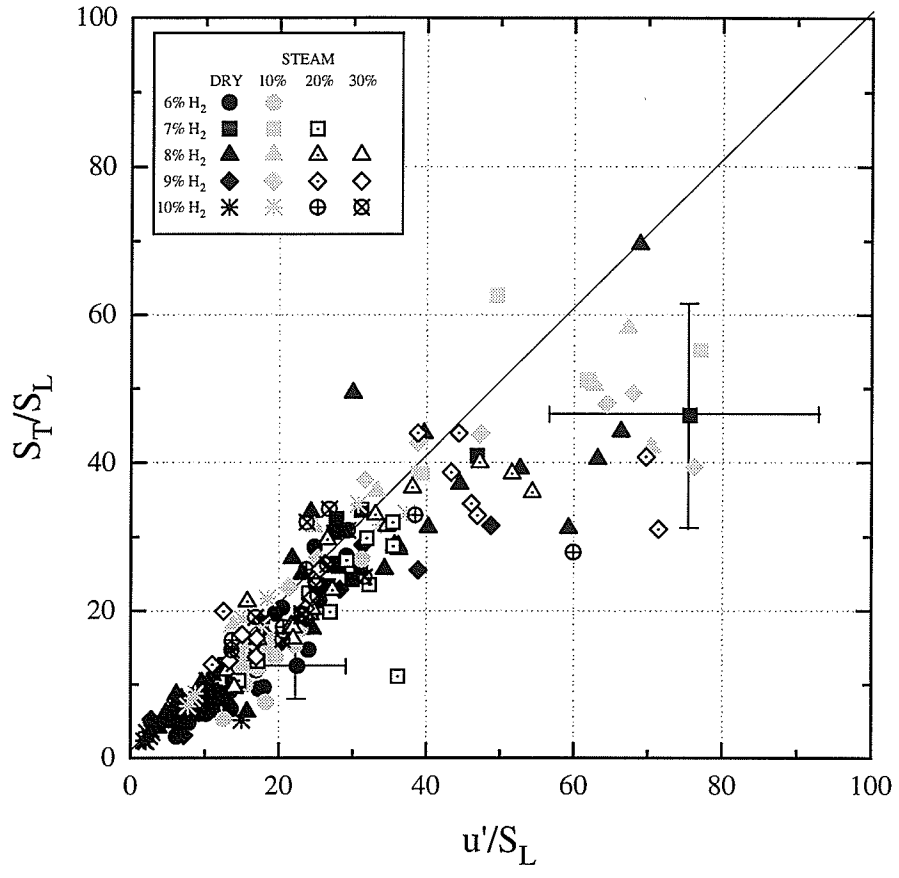
Figure 5.3: Normalized turbulent burning velocity versus normalized fluctuating turbulent velocity for all mixtures. Typical error bars are shown.
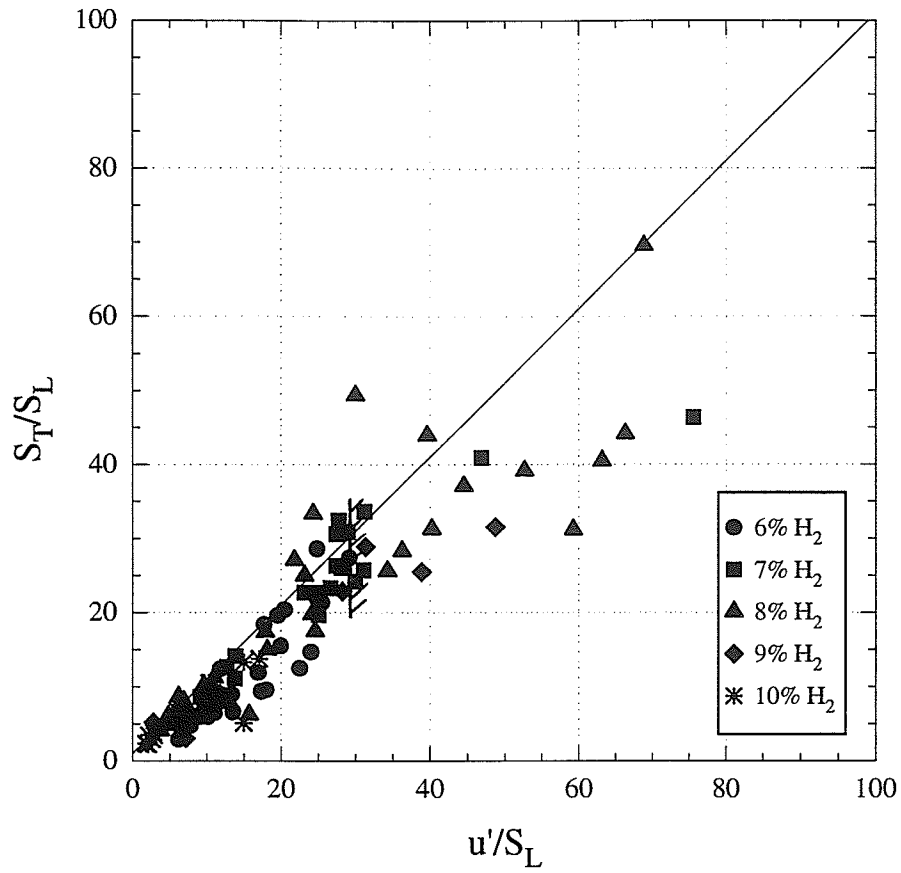
Figure 5.4: Normalized turbulent burning velocity versus normalized fluctuating turbulent velocity for dry mixtures at room temperature.
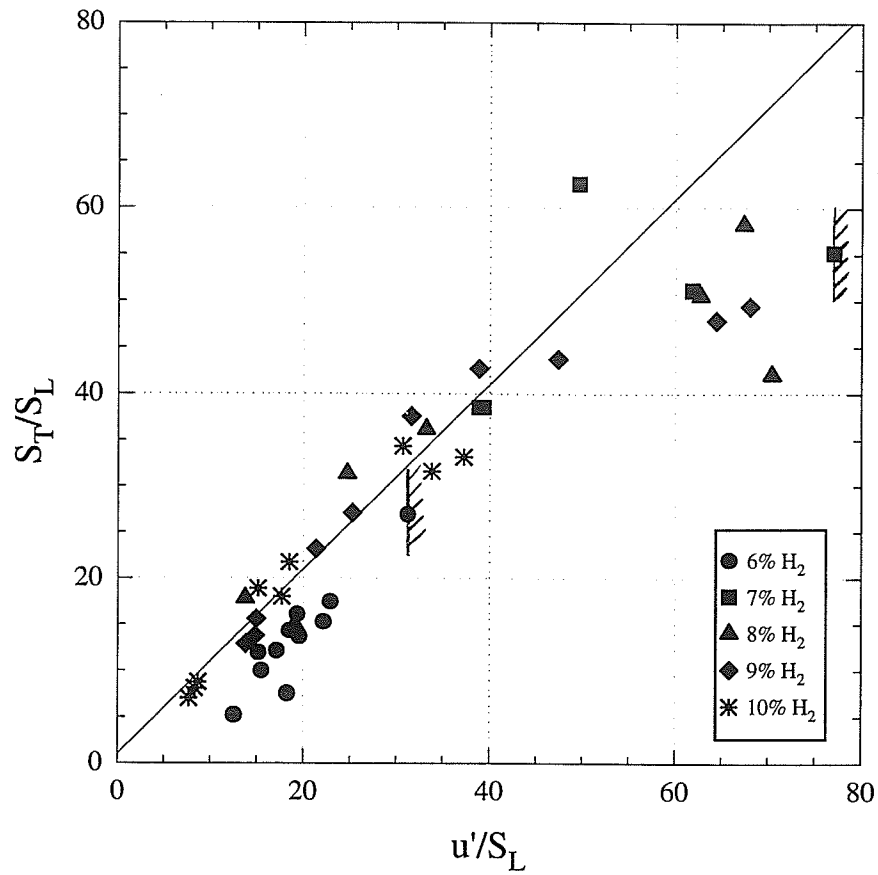
Figure 5.5: Normalized turbulent burning velocity versus normalized fluctuating turbulent velocity for 10% steam mixtures.
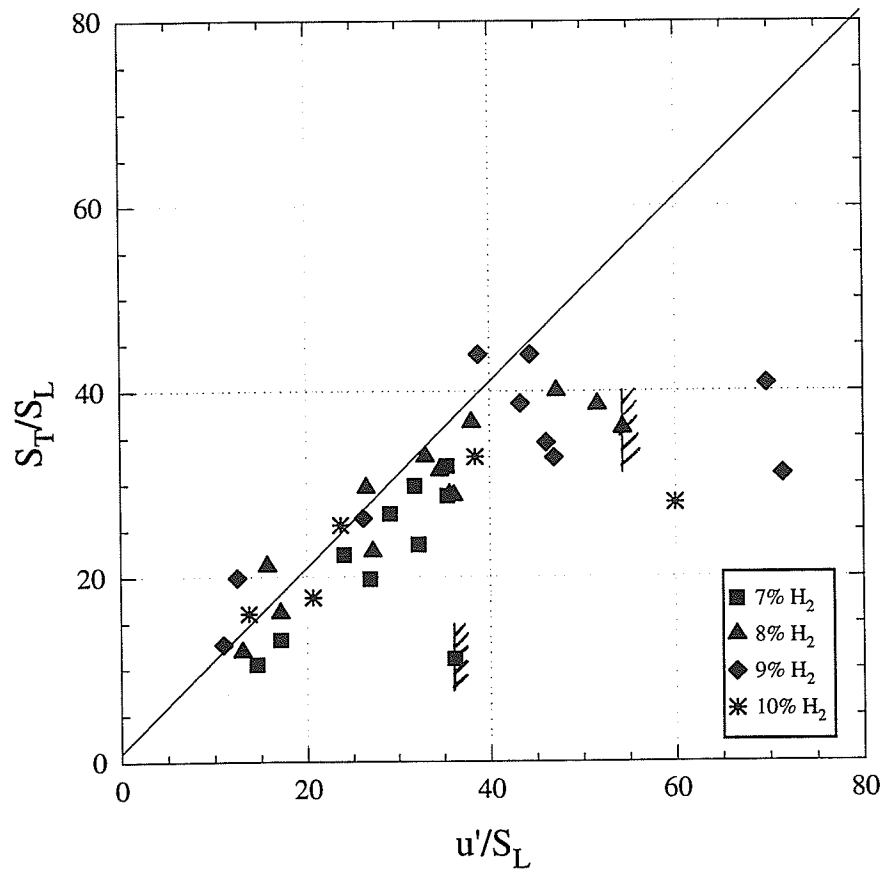
Figure 5.6: Normalized turbulent burning velocity versus normalized fluctuating turbulent velocity for 20% steam mixtures.
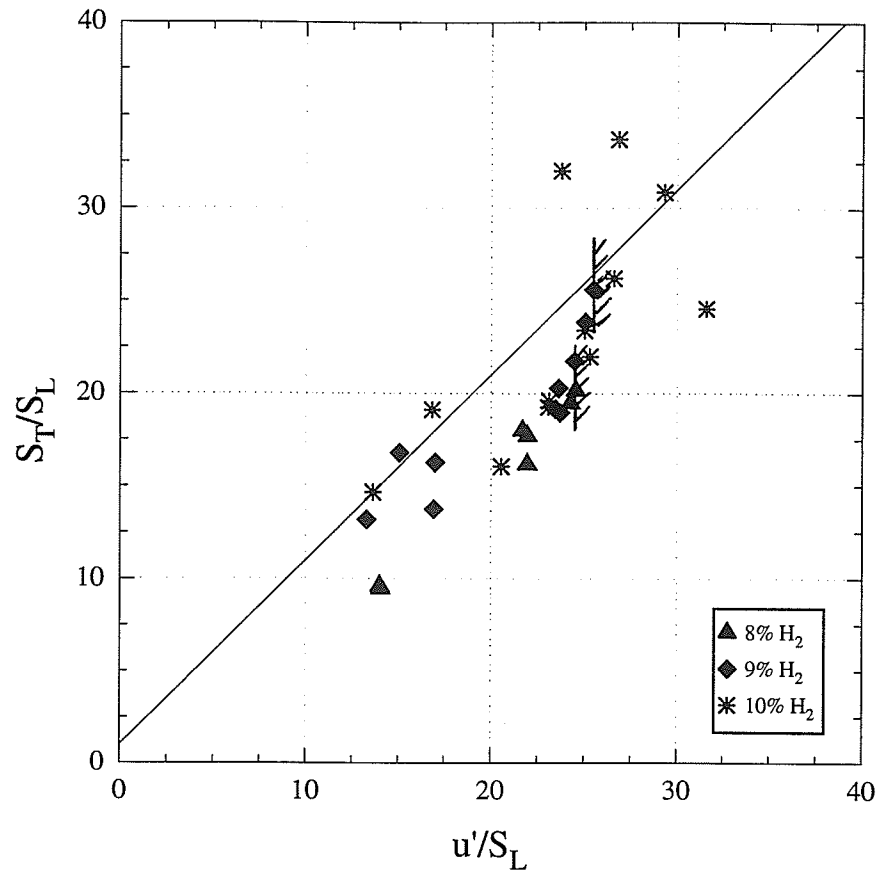
Figure 5.7: Normalized turbulent burning velocity versus normalized fluctuating turbulent velocity for 30% steam mixtures.
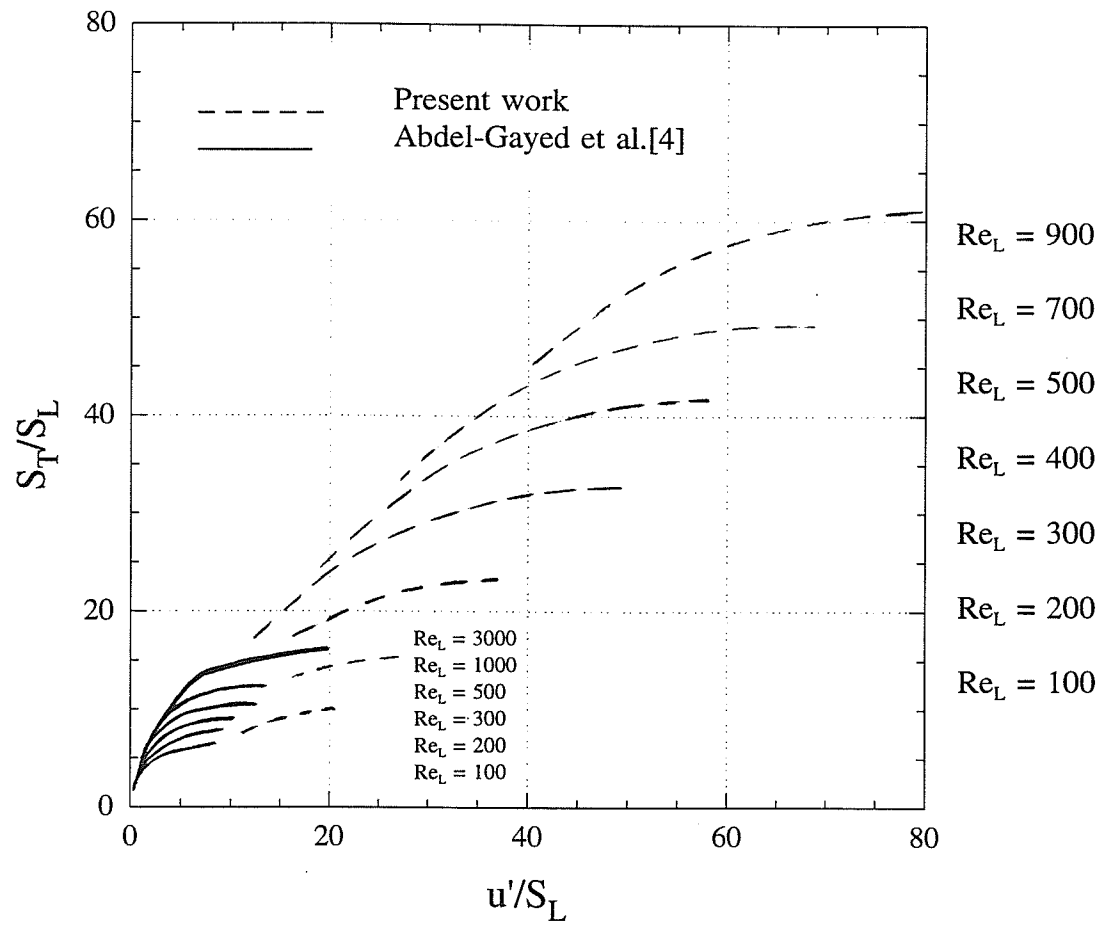
Figure 5.8: The flame law from the present work and the correlations from Abdel-Gayed et al. [4].
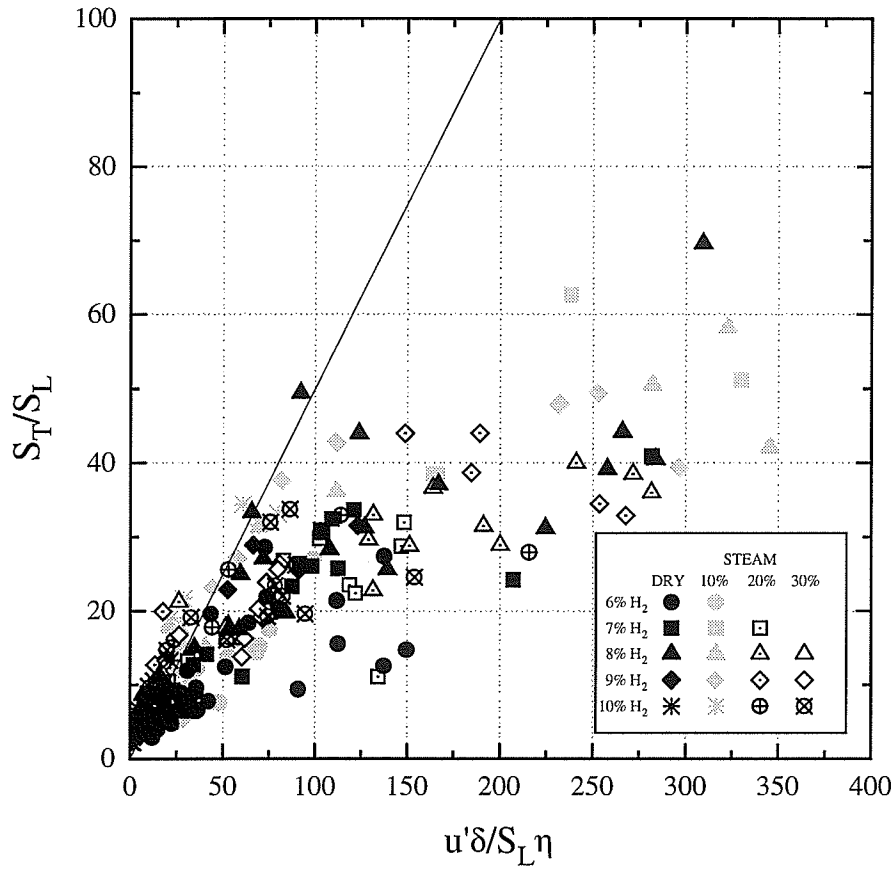
Figure 5.9: H$_2$-air-steam data from the present work compared to the relation of Ballal and Lefebvre. [9].

6.0 SUMMARY

Turbulent burning of near-flammability-limit H_2-air-steam mixtures was examined under various turbulent environments. Turbulence was generated by pulling a perforated plate across the combustion chamber. Turbulence parameters were determined by making x-wire anemometry measurements behind a similar perforated plate in a wind tunnel. Effective laminar and turbulent burning velocities were calculated using the early pressure-time history of the burn inside the combustion chamber. Burning velocity data collected for 6-10% H_2-air-steam flames in various turbulent conditions were compared to correlations by other researchers. The data showed that turbulent enhancement of burning velocity is strongly affected by mixture sensitivity, since lean H_2-air-steam flames showed more enhancement for a given turbulent Reynolds number than the near-stoichiometric mixtures used in Abdel-Gayed et al.'s[4] correlations. The comparison to Ballal and Lefebvre's[9] results showed that the correlation they used to describe highly turbulent combustion cannot be used to describe the results of this paper. Examining the data in terms of normalized turbulent burning velocities versus normalized turbulent fluctuating velocities demonstrated that using the wrinkled flame law (a linear relationship) to describe the enhancing effect of turbulence on burning rate is acceptable for near-flammability-limit mixtures. The data began to depart from the wrinkled flame law at high turbulence levels, which is a trend seen by other researchers near quenching conditions. Finally, critical turbulence levels were found for some insensitive mixtures, beyond which no burning was observed.

7.0   SUGGESTED FUTURE WORK

It is suggested that further experiments be performed to verify that the critical turbulence levels are actually caused by flames being quenched by high turbulence levels, and not caused by ignition problems. This could be done by increasing the spark energy level and by taking schlieren photographs of the burns near and at quenching conditions.

As well, experiments at higher turbulence levels would verify whether the burning velocity data does depart from the wrinkled flame law or whether the increased uncertainty in the turbulence intensities caused this trend. This would require modifying the turbulence generating apparatus, as it cannot presently produce higher turbulence levels.

Finally, it would be interesting to study the effect of length scale on combustion by systematically varying the length scales. This could be done by using plates with different hole sizes.

REFERENCES

1.   Abdel-Gayed, R. G., and Bradley, D., "A Two-Eddy Theory of Premixed Turbulent Flame Propagation." Philosophical Transactions of the Royal Society of London, A301, p. 1-25, 1981.

2.   Abdel-Gayed, R. G., Al-Khishali, K. J., and Bradley, D., "Turbulent burning velocities and flame straining in explosions." Proceedings of the Royal Society of London, A391, p. 393-414, 1984.

3.   Abdel-Gayed, R. G., Bradley, D., and Lawes, M., "Turbulent Burning Velocities: a General Correlation in Terms of Straining Rates." Proceedings of the Royal Society of London, A414, p. 389-413, 1987.

4.   Abdel-Gayed, R. G. and Bradley, D., and Lung, F. K.-K., "SHORT COMMUNICATION: Combustion Regimes and the Straining of Turbulent Premixed Flames." Combustion and Flame, Vol. 76, p. 213-218, 1989.

5.   Al-Khishali, K. J., Bradley, D., and Hall, S. F., "Turbulent Combustion of Near-Limit Hydrogen-Air Mixtures." Combustion and Flame, Vol. 54, p. 61-70, 1983.

6.   Andrews, G. E., and Bradley, D., Combustion and Flame, Vol. 20, p. 77, 1973. (As reported in [23]).

7.   Andrews, G. E., and Bradley, D., "Turbulence and Turbulent Flame Propagation-A Critical Appraisal." Combustion and Flame, Vol. 24, p. 285-304, 1975.

8.   Baines, W. D., and Peterson, E. G., "An Investigation of Flow Through Screens." Transactions of the ASME, Vol. 73, p. 467, 1951.

9.   Ballal, D. R., and Lefebvre, A. H., "The Structure and Propagation of Turbulent Flames." Proceedings of the Royal Society of London, A344, 1975.

10.   Berman, M., Sandia Laboratories Report, SAND84-0689, 1984. (As reported in [23]).

11.   Bradbury, L. J. S., "Measurements with a Pulsed-Wire and a Hot-Wire Anemometer in the highly turbulent wake of a normal flat plate." Journal of Fluid Mechanics, Vol. 77, p. 473-497, 1976.

12.   Bradley, D., Lau, A. K. C., and Lawes, M., "Flame stretch as a determinant of

turbulent burning velocity." Philosophical Transactions of the Royal Society of London, A338, p. 359-387, 1992.

13.   Checkel, M. D., "Measurements of Turbulence Generated by 60 Percent Solid Perforated Plates." Journal of Fluids Engineering, Vol. 108, p. 55-63, March 1986.

14.   Checkel, M. D., and Thomas, A., "Turbulent Explosions in Closed Vessels." The Institution of Mechanical Engineers Conference on Combustion in Engineering, paper C57/83, 1983.

15.   Checkel, M. D., and Ting, D. S-K., "Turbulence Effects on Developing Turbulent Flames in a Constant Volume Combustion Chamber." SAE Technical Paper 9308667.

16.   Checkel, M. D., and Ting, D. S-K., "Measuring Turbulent Flame Growth by Visualization." 1992 SAE International Congress & Exposition, paper 920184, Feb. 1992.

17.   Comte-Bellot, G., and Corrsin, S., "The use of a contraction to improve the isotropy of grid-generated turbulence." Journal of Fluid Mechanics, Vol.25, part 4, p. 657-682, 1966.

18.   Dahl, H. J., *Calibration of a Wind Tunnel Test Section for a Boundary Layer Wake Mixing Experiment*. B.Sc. thesis, Mechanical Engineering Department, University of Manitoba, April, 1987.

19.   Gaydon, A. G., and Wolfhard, H. G., *Flames: their structure, radiation, and temperature*. London:Chapman and Hall, 1970.

20.   Hinze, J. O., *TURBULENCE: An Introduction to Its Mechanism and Theory*. Toronto:McGraw-Hill Book Company Inc., 1959.

21.   Incropera, F. P., and De Witt, D. P., *Fundamentals of Heat and Mass Transfer*. 3rd edition, New York:John Wiley and Sons, 1990.

22.   Johnson, F. D., and Ecklemann, H., "A variable angle method of calibration for X-probes applied to wall-bounded turbulent shear flow." Experiments in Fluids, Vol. 2, p. 121-130, 1984.

23.   Koroll, G. W., Kumar, R. K., and Bowles, E. M., "Burning velocities of Hydrogen-air Mixtures." Combustion and Flame, Vol. 94, p. 330, 1993.

24.   Lewis, B., and von Elbe, G., *Combustion, Flames and Explosions of Gases.*

2nd ed., New York:Academic Press, 1961.

25.   Lueptow, R. M., Breuer, K. S., and Haritonidis, J. H., "Computer-aided
        calibration of X-probes using a look-up table." Experiments in Fluids, Vol. 6,
        p. 115-118, 1988.

26.   McDonell, B. J., *Burning Rates of Propane-Air Mixtures in Homogeneous
        Decaying Turbulence*. M.Sc. Thesis, Mechanical Engineering Department,
        University of Alberta, 1988.

27.   Moffat, R.J., "Describing the Uncertainties in Experimental Results."
        Experimental Thermal and Fluid Science, Vol. 1, p. 3-17, 1988.

28.   Rallis, C. J., and Garforth, A. M., "The Determination of Laminar Burning
        Velocity." Progress in Energy Combustion Science, Vol. 6, p. 303-329, 1980.

29.   Tennekes, H., and Lumley, J. L., *A First Course in Turbulence*. Cambridge,
        Massachusetts:Massachusetts Institute of Technology, 1972.

30.   Townsend, A. A., *The Structure of Turbulent Shear Flow*. 2nd ed.,
        Cambridge:Cambridge University Press, 1976.

31.   Uberoi, M. S., and Wallis, S., "Effect of Grid Geometry on Turbulence Decay."
        The Physics of Fluids, Vol. 10, No. 6, p. 1216, 1967.

32.   Watson, J. T. R., "Viscosity of Gases in Metric Units." National Engineering
        Library, Edinburgh:Her Majesty's Stationary Office, 1972.

33.   Wilke, C.R., "A Viscosity Equation for Gas Mixtures." Journal of Chemical
        Physics, Vol. 18, No. 4, p. 517, 1950.

34.   "Science and Engineering Tools for Microsoft Fortran: IPC-MF-006 Version
        6.1", Quinn-Curtis.

APPENDIX A: Turbulence measurements in the wind tunnel

A.1   Calibration

Turbulence measurements were made in a closed-loop low turbulence wind tunnel with a test section of 0.53 m x 0.76 m blocked by perforated plates. The wind tunnel is driven by two contra-rotating 1.2 m diameter fans powered by two fixed displacement hydraulic motors. A schematic of the wind tunnel is shown in Figure A.1. Four corner fillets taper in the direction of the flow, causing a slight increase in the test section's cross-sectional area to compensate for the boundary layer growth along the walls. The perforated plates used to produce the turbulence have the same thickness, hole size, and spacings as the 0.12 m x 0.12 m plates used in the combustion chamber. Wind tunnel velocities in the empty test section were calculated by dividing the pressure drop, ΔP_d, across the diffuser by 1.04. This coefficient was calculated by comparing the pressure differential across the diffuser to that of the pitot-static tube in the test section. It was originally calculated by Dahl[18] as 1.0874, and was recalculated for the present work. Placing the plates in the wind tunnel changed the pressure drop-flow rate characteristic of the wind tunnel and therefore also changed the coefficient. Pitot-tube measurements in the up and down direction (from here on called the $\pm$ y-direction or the transverse direction) show that there is a 10 cm central region behind the plate where the velocity is constant. By assuming that the flow is essentially two-dimensional, this means that there is a 0.1 m $\times$ 0.1 m central constant-velocity area behind the plate. All anemometry measurements in both the streamwise and transverse directions were made within this constant-velocity area.

Measurements were made by a tungsten x-wire with a sensor diameter of 5 μm and sensor length of 1 mm, giving an aspect ratio of 200. The output of the Disa 55M01 constant temperature bridge was sent to a Disa 55M25 linearizer, then recorded using a DAS-1600 data-acquisition board installed in a 386 PC. The frequency response of the x-wires was determined by the standard square wave test. The sampling frequency for the tests was determined by making measurements at several sampling speeds, and

finding the frequency at which the calculated parameters ($\overline{uv}$ correlation, and skewness and flatness factors), were no longer affected by the sampling speed. This value was 25 kHz. (Note: the sampling speed used by Checkel[13] and McDonell[26] behind similar perforated pates was 20 kHz).

The probe used in this study was calibrated according to the method described in Lueptow et al.[25], and Johnson and Ecklemann[22]. The x-wire probe was pitched through several angles with respect to the calibration flow, for several flow velocities. A unique voltage pair (E1,E2) was measured for each pitch angle, γ, and flow velocity Q. In contrast to Johnson and Ecklemann, who found unique voltage pairs only for $\gamma = \pm 30°$, unique voltage pairs were found for $\gamma = \pm 40°$ for the x-wire probe used in these experiments. Typical calibration output (E1 vs. E2) is shown in Figure A.2. From the calibration data, a look-up table was created. A computer program was used to search the look-up table, match voltage pairs to a unique flow rate and flow angle, and convert the flow rate and angle to velocities. The instantaneous velocities $\tilde{u} = Q*\cos(\gamma)$ and $\tilde{v} = Q*\sin(\gamma)$ were used to calculate the mean and r.m.s. turbulent velocities as well as the skewness and flatness factors and the $\overline{uv}$ correlation. The listing of the computer code is included in Appendix C. In the highly turbulent region near the plate, voltage pairs were recorded which did not fit into the look-up table. For all streamwise measurements, these "bad" data did not exceed 0.6% of the total number of samples. The highest number of "bad" points were seen in the transverse measurements at one and two hole diameters away from the plate, up to 1.9% of the total number of samples. The effect of these "bad" data were considered insignificant compared to other experimental uncertainties and were ignored.

The x-wire probe was calibrated in the empty wind tunnel test section. This ensured that the calibration would not change in the move from calibration set-up to measurement set-up. Background turbulence measurements in the wind tunnel with no plate present indicated streamwise turbulence intensities of $u'/\overline{U} = 0.005$ at air speeds of 10 m/s and 5 m/s. This background turbulence was considered insignificant

43

compared to the high turbulence created by the perforated plate.

Ideally, all streamwise measurements should be made with the hot-wire probe carefully aligned with the centreline of a hole. Unfortunately, constraints did not allow this and measurements were made with the probe positioned 1/3 of a radius from the centreline. This misalignment is only expected to affect the results near the perforated plate, since the jets of air flowing through the holes quickly break down into homogeneous turbulence.

Figure A.3 shows the ratio of measured average streamwise velocity, $\bar{U}_i$, to the reference average streamwise velocity (at x/D=20), $\bar{U}_{ref}$, plotted against non-dimensionalized distance from the plate, x/D. Both the 10 mm and 5 mm plates show excellent agreement between x/D=10 and x/D=50. The 20 mm plate shows some decrease in the measured velocity starting at x/D=35. This is the opposite trend expected from a centreline velocity affected by a wall boundary layer. Therefore, it is most likely due to unavoidable physical maneuvering that occurred during the test and not to some characteristic of the flow itself. It was not observed in earlier test results. The probe holder is moved in the streamwise direction using slots in a plexiglass panel in the ceiling of the wind tunnel test section. This panel does not extend the entire length of the test section, however, and the panel itself must be moved and exchanged with another panel when measurements farther than 80 cm downstream of the plate need to be taken. This requires turning off the wind tunnel. Both the change in air temperature caused by turning off the wind tunnel, the uncertainty in achieving the exact same air speed when restarting the wind tunnel, and the possible jolting of the probe during the movement of the panel could cause discontinuities in the measurements from one position to another. Measurements for the 5 mm plate were all performed with the panel in one position. The 10 mm plate required that the panel be moved once, to get the last three downstream positions, x/D=45, 50, and 60. For measurements with the 20 mm plate, the panel needed to be moved twice, at x/D=35 and at x/D=45. These downstream positions correspond to increasing disagreement in

44

the output. The output of the 20 mm and 10 mm plates is therefore ignored for x/D>30 and x/D>40, respectively.

The reliability of hot-wire anemometry at high turbulence intensities (>20%) is suspect because hot-wire measurements give erroneously high values for the mean velocity and low values for the fluctuating velocities. Therefore Bradbury's[11] correction factors, valid for turbulence intensities up to approximately 50%, are used. The correction factors are only applied for x/D≥5 because close to the plate, the measured turbulence intensities are higher than 50%.

A.2   Experimental Uncertainty

The estimated experimental uncertainties for the turbulence results are based on repeatability and the bias of $\overline{V}$ from 0 m/s (due to misalignment of the probe). The uncertainties are propagated for u' and v' and the higher order moments using the Root-Sum-Square method. This method is likely very conservative, especially for the higher order moments. The uncertainties are shown in Table A.1.

Table A.1   Experimental uncertainty in the turbulence parameters

Parameter	Uncertainty	
	u	v
mean velocity	7%	0.252m/s
r.m.s. velocity	10%	0.356m/s
skewness factor	42%	1.07m/s
flatness factor	57%	1.42m/s
$\overline{uv}$ correlation	0.253m/s	

45

A.3   Measurements

Figure A.4 shows the average and r.m.s. fluctuating velocities measured by moving the hot-wire probe in a straight line vertically between hole centres. Because of the symmetry of the hole configuration and the expected corresponding symmetry of the turbulence, the measurements were taken only from the hole centre to a transverse distance of 30 mm. The results were then repeated in the transverse direction to create Figure A.4. At one hole diameter (x/D=1) downstream of the plate, a strong jet exits each hole. Turbulence levels are higher at the edges of these jets than at the centre because the edges of the jet are interacting with the slower fluid, creating eddies. At x/D=2 and x/D=4, the jet velocity decreases and the average velocity increases. By x/D=6, the jets have nearly disappeared and the average and turbulent velocities have levelled out. At x/D=10, there is no trace of the jets in the velocity profiles. Because of the slight misalignment of the probe, the results probably show that the jets disappear slightly earlier than they actually do, otherwise, the general trends observed should be correct. Conservation of mass is observed to within 5% between x/D=1 and x/D=10.

Figure A.5 shows v'/u' versus distance from the plate, which is an indication of the isotropy of the turbulence. The average value of the ratio is 0.9, which indicates that the turbulence is close to isotropy. This value compares well to values for grid-generated turbulence found by other researchers. Uberoi and Wallace[30] found values between 0.75 and 0.95, while Comte-Bellot and Corrsin[17] found values between 0.9 and 0.95.

Figures A.6 and A.7 show the power density functions of the instantaneous velocities compared to the corresponding Gaussian distribution, at two distances downstream of the plate. The pdf at x/D=30 agrees well with the Gaussian distribution and the calculated u-skewness factor of 0.07 and v-skewness factor of -0.04. The pdf at x/D=5 is skewed, which is expected since the jets have not completely broken down

into homogeneous turbulence this close to the plate. The corresponding u-skewness factor is 0.58 and the v-skewness factor is 0.29.

Figure A.8 shows the skewness factor versus distance from the plate. A Gaussian distribution should have a skewness of zero, and far downstream of the plate, the skewness remains within ± 0.25. Figure A.9 shows the flatness factor versus distance from the plate. A Gaussian distribution should have a flatness factor of three. Far downstream from the plate, the measured flatness factor equals 3.0 ± 0.25. The uncertainty calculated in the previous section is likely very conservative, because it is much larger than the variations shown in the results.

Figure A.10 shows the $\overline{uv}$ correlation versus distance from the plate. The $\overline{uv}$ correlation value should be zero in isotropic turbulence. This flow is only approximately isotropic, however, as can be seen in the gradual increase in the $\overline{uv}$ correlation with increasing distance from the plate.
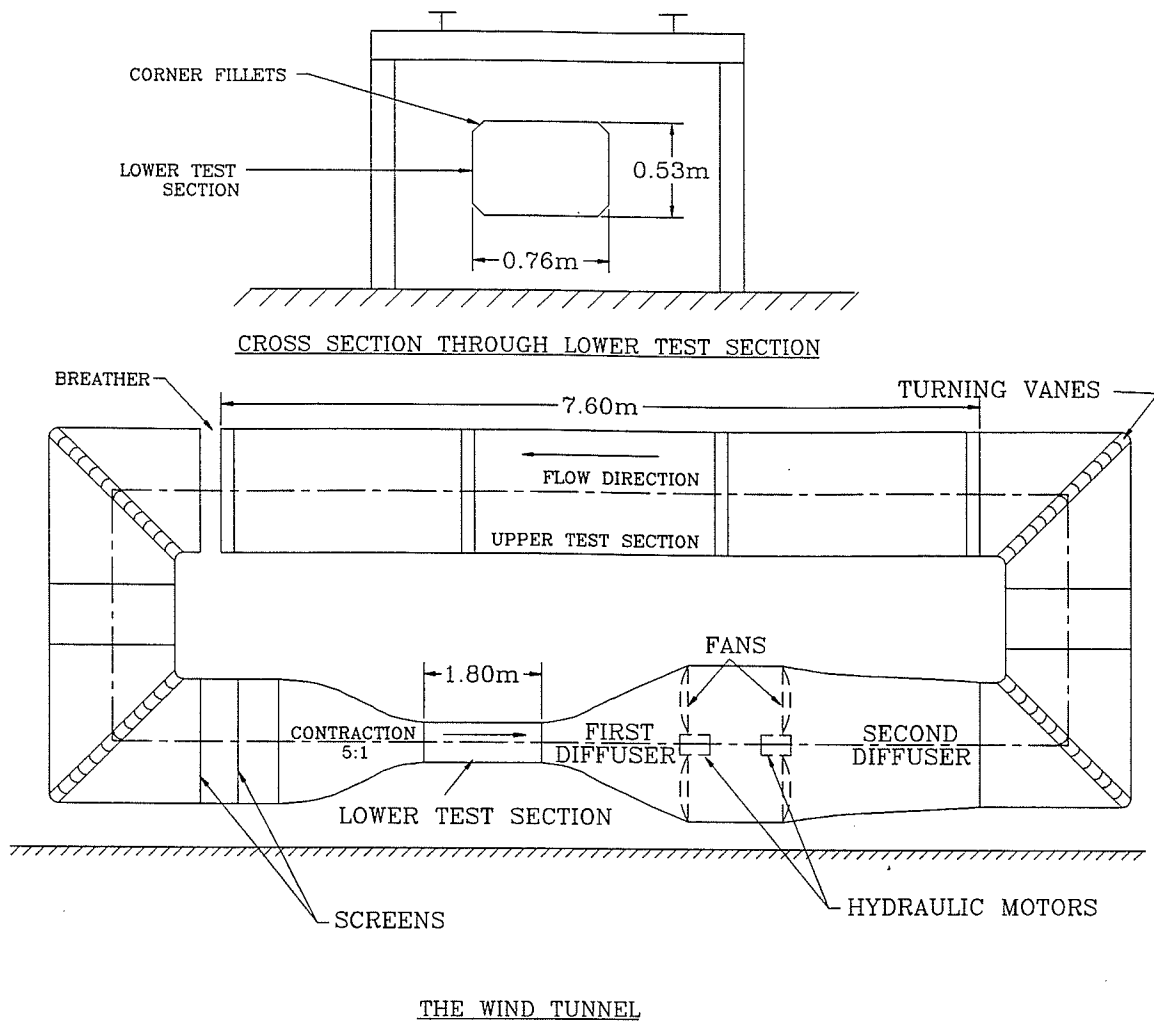
CORNER FILLETS

LOWER TEST
SECTION

0.53m

←0.76m→

CROSS SECTION THROUGH LOWER TEST SECTION

BREATHER

←————————7.60m————————→

TURNING VANES

FLOW DIRECTION

UPPER TEST SECTION

FANS

←1.80m→

CONTRACTION
5:1

FIRST
DIFFUSER

SECOND
DIFFUSER

LOWER TEST SECTION

SCREENS

HYDRAULIC MOTORS

THE WIND TUNNEL

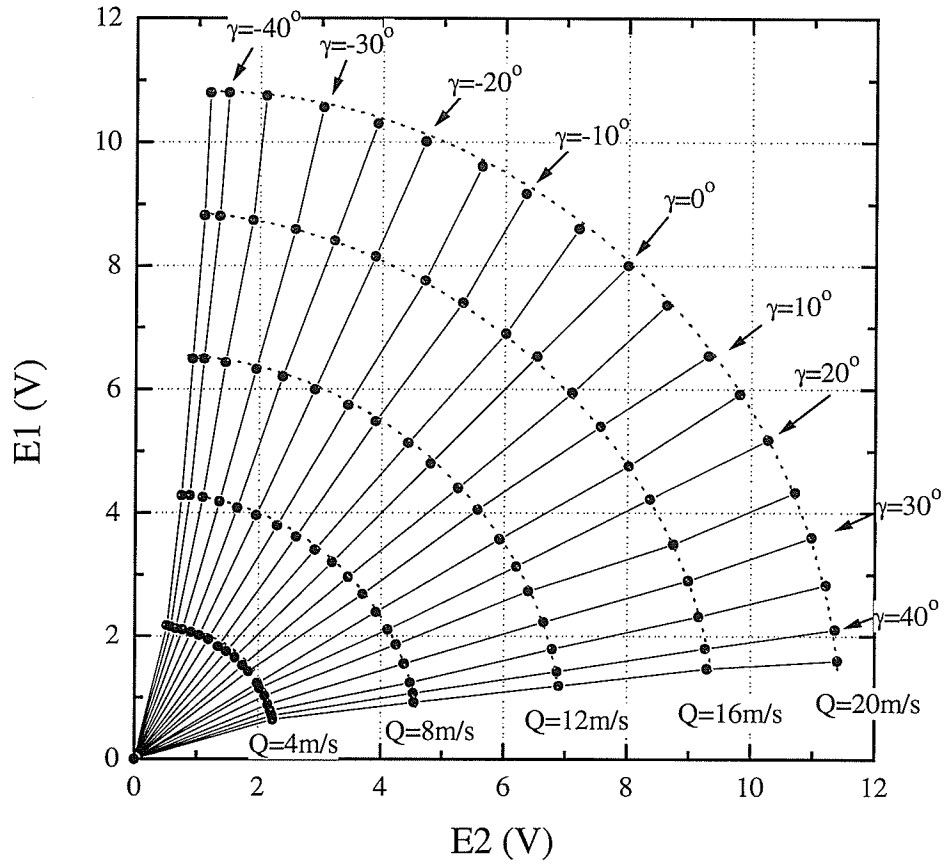**Figure A.1:** **Schematic of the wind tunnel.**

Figure A.2: Typical calibration data for the x-wire anemometer. E1 and E2 are the output voltages from each wire.
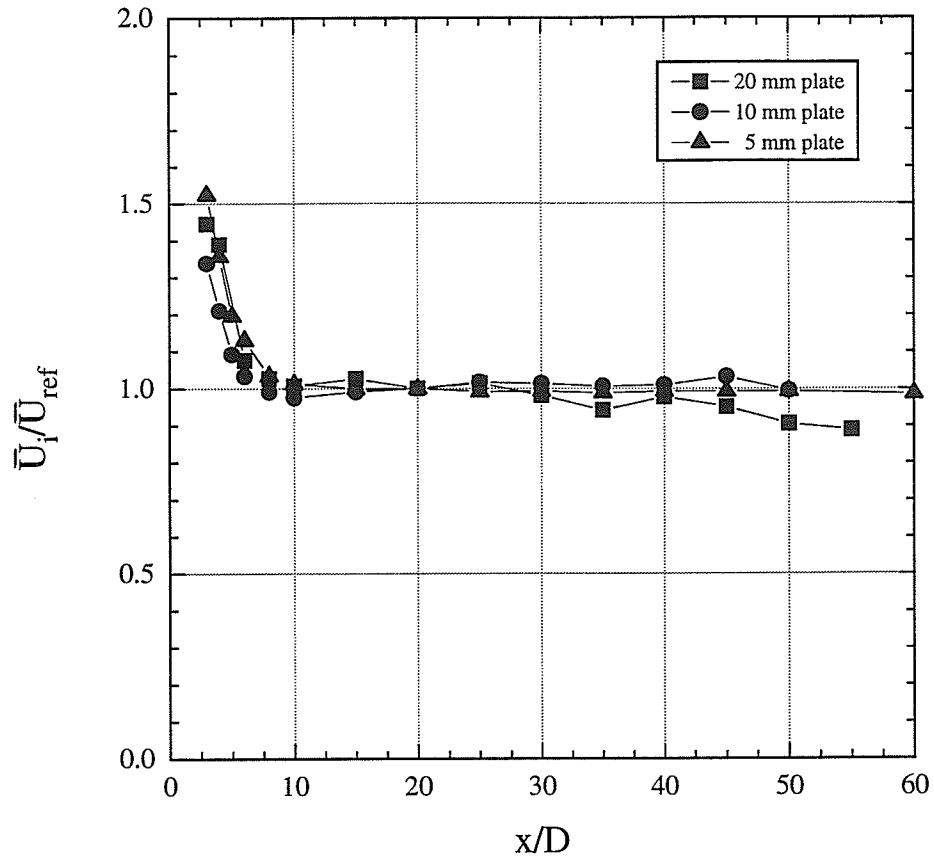
Figure A.3   Local average streamwise velocity normalized by a reference average streamwise velocity versus distance from the plate.
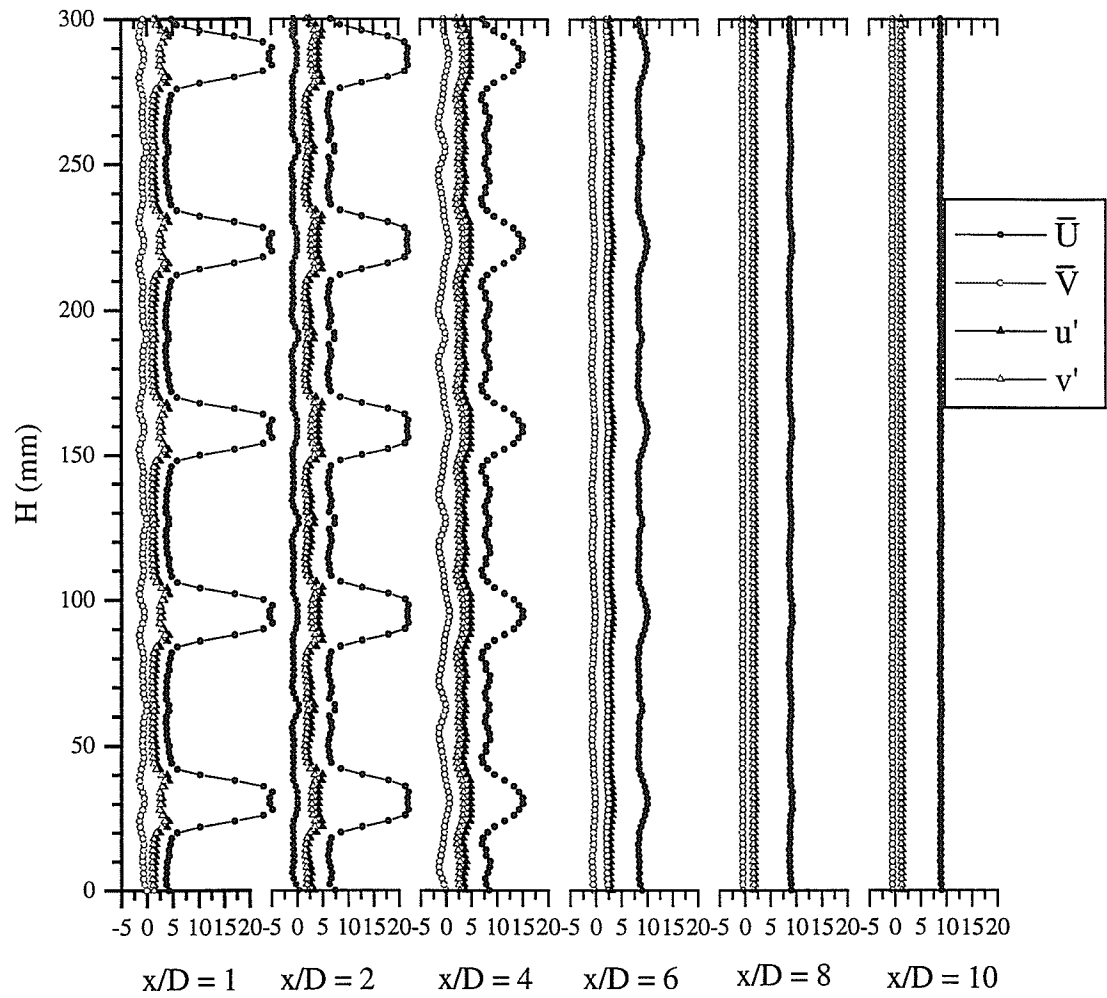
Figure A.4   Transverse velocity profiles behind the 20 mm diameter hole plate.
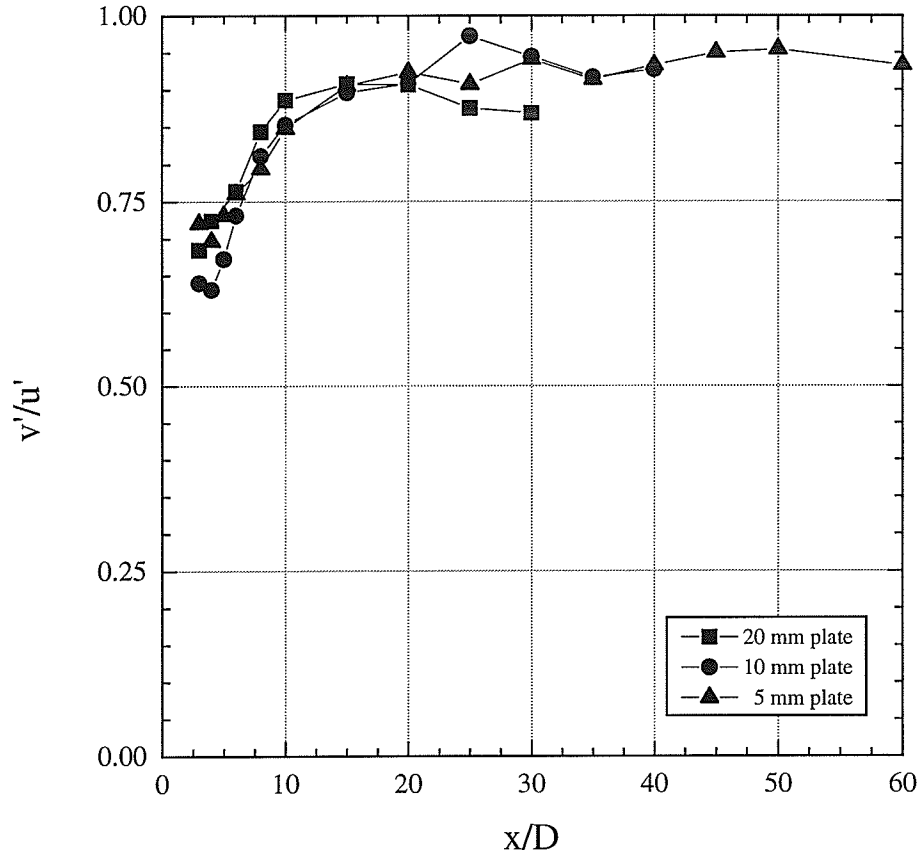
Figure A.5   The ratio of transverse to streamwise r.m.s. turbulent velocity, v'/u' versus distance from the plate.
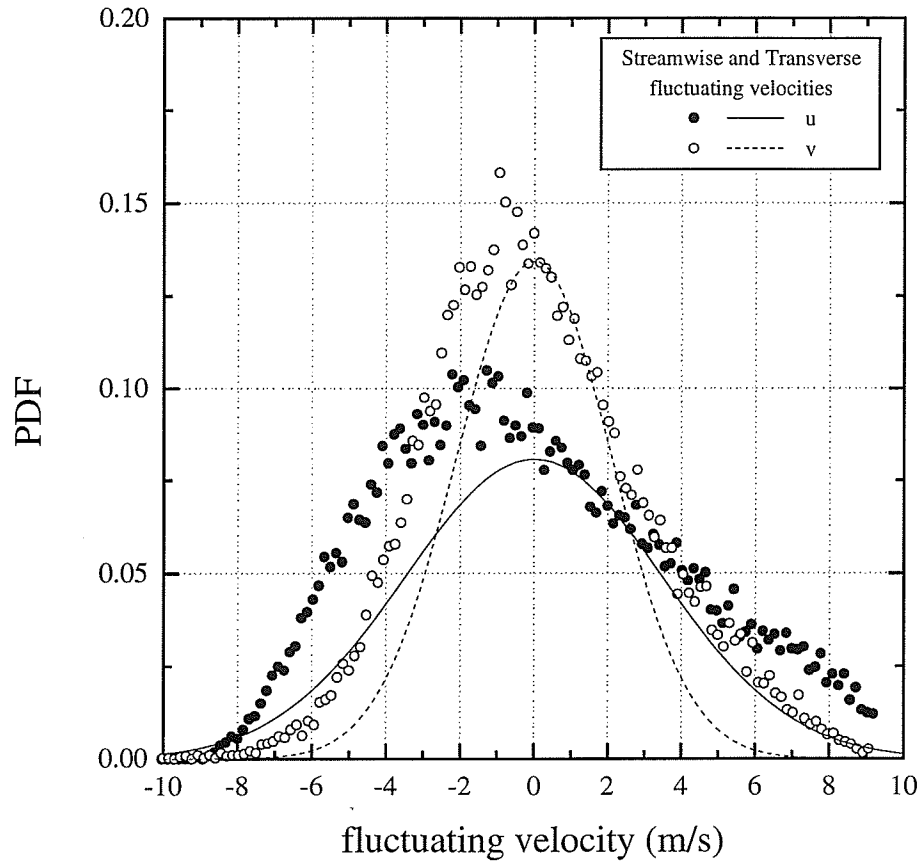
Figure A.6 PDF of streamwise and transverse fluctuating velocities at x/D=5, u-skewness factor=0.58. Solid and dashed lines are the corresponding Gaussian distributions.
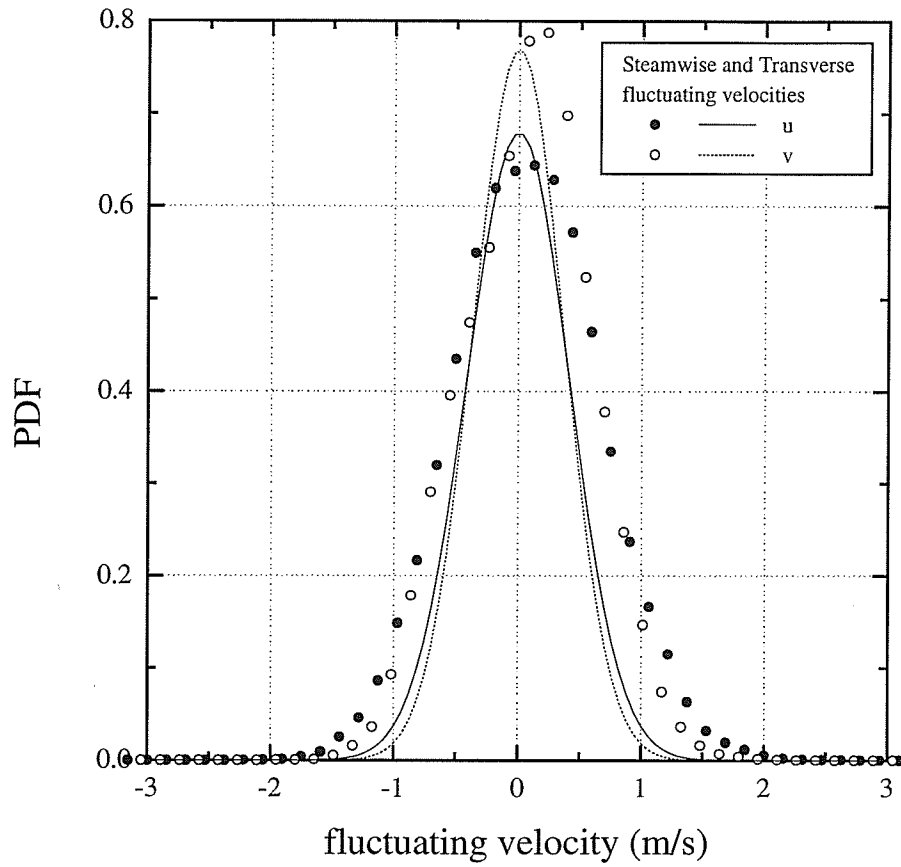
Figure A.7 **PDF of streamwise and transverse fluctuating velocities at x/D=30, u-skewness factor=0.08. Solid and dashed lines are the corresponding Gaussian distributions.**
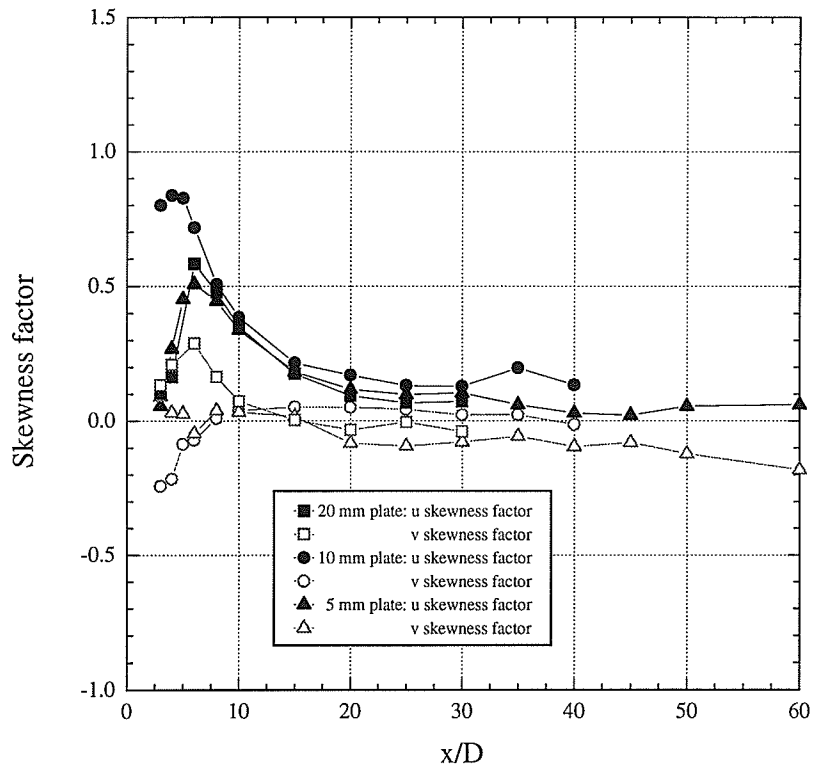
Figure A.8   Skewness factor versus distance from the plate.
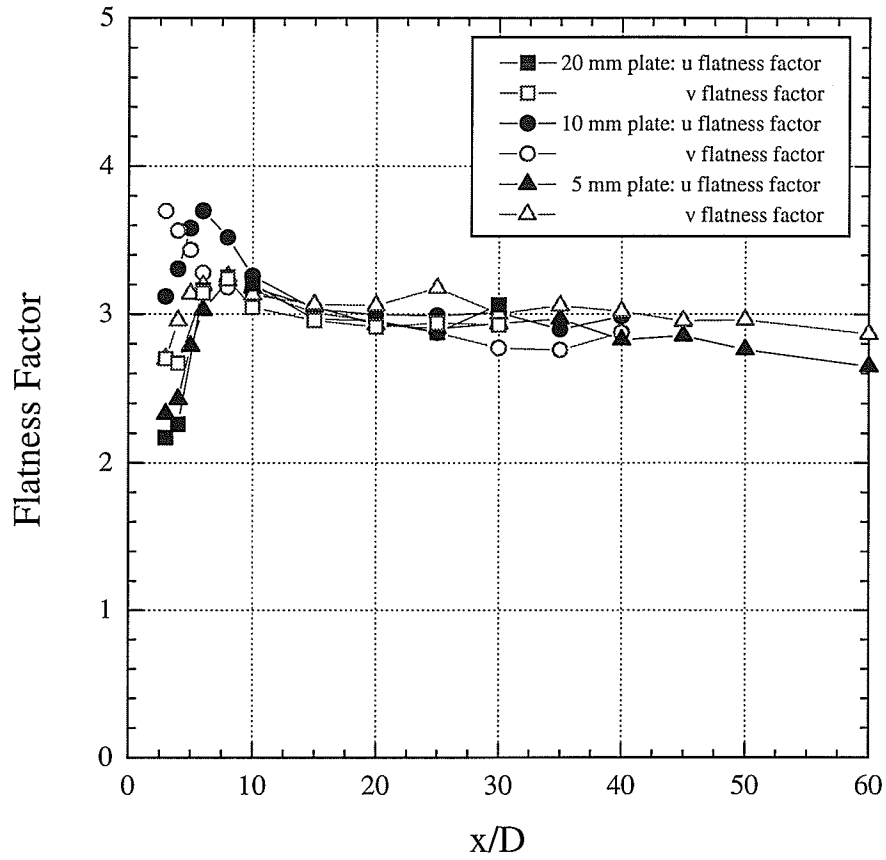
Figure A.9   Flatness factor versus distance from the plate.
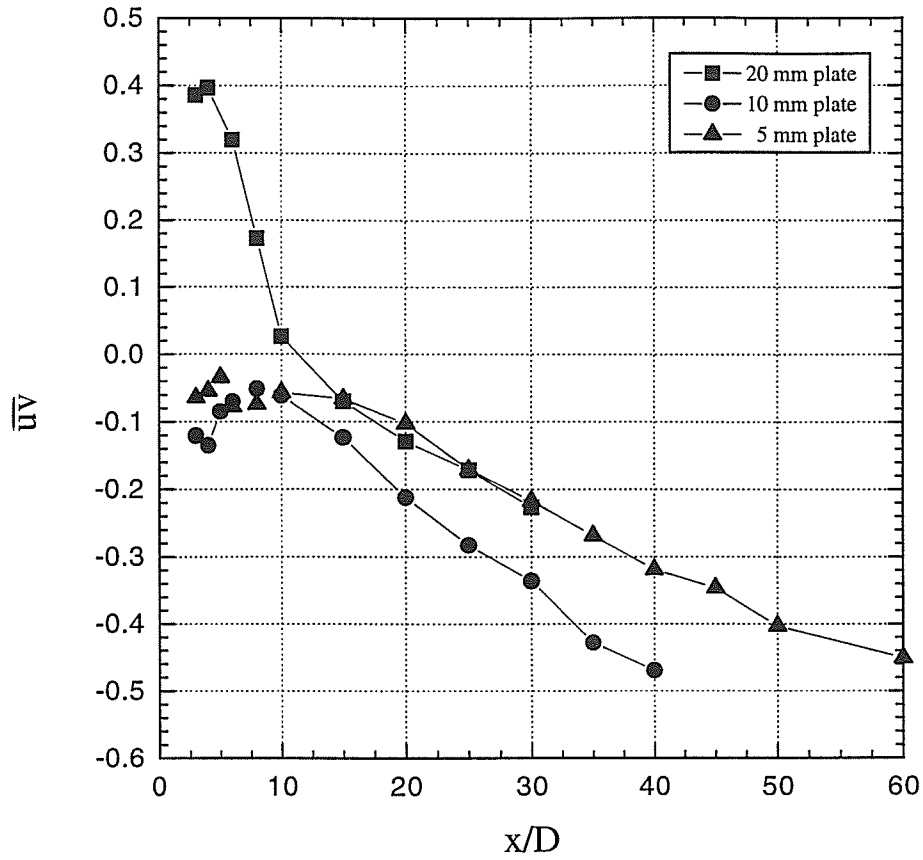
Figure A.10 Transverse-streamwise velocity correlation versus distance from the plate.

APPENDIX B: A method for calculating the effective burning velocity of a premixed flame from a pressure trace.

A Method for Calculating the Effective Burning Velocity
of a Premixed Flame

Assumptions:

1. Spherical flame kernel, so that

$$V_b = \frac{4}{3} \pi R_f^3 \quad , \quad A_f = 4 \pi R_f^2$$

V_b = volume of burnt gas
R_f = flame radius
A_f= flame surface area

2. Fraction of mass burned equals the fraction of the total adiabatic constant volume combustion pressure rise

$$\frac{m_b}{m_o} = \frac{P - P_o}{P_{cv} - P_o}$$

m_b = mass of the burnt gas
m_o = mass of the total original unburnt gas
P_o = starting pressure
P_{cv} = constant volume combustion pressure
P = pressure

3. The law of adiabatic compression:

$$\frac{P}{\rho^\gamma} = constant \quad \Rightarrow \quad \frac{d\rho_b}{dt} = \frac{\rho_b}{\gamma_b P} \frac{dP}{dt}$$

ρ = density
γ = specific heat
subscripts u and b refer to the unburnt
and burnt gases, respectively.

59

4. At P_o, no burned gas is present, so we must assume that

$$\frac{\rho_b{}^{\gamma_b}}{\rho_{b,o}{}^{\gamma_b}} = \frac{P}{P_o}$$

$\rho_{b,o}$ = the density of the burned gas at P_o.

Conservation of mass

$$m_b + m_u = m_o \quad \Rightarrow \quad \frac{dm_b}{dt} = -\frac{dm_u}{dt}$$

For a constant volume combustion chamber:

$$V_b + V_u = V_o \quad \Rightarrow \quad \frac{dV_b}{dt} = -\frac{dV_u}{dt}$$

m_u and V_u = the mass and volume of the unburnt gas.
m_b and V_b = the mass and volume of the burnt gas.
V_o = the initial volume of total gas. Also the vessel volume.

Analysis:

$$\frac{dm_b}{dt} = \frac{d(\rho_b V_b)}{dt} = V_b \frac{d\rho_b}{dt} + \rho_b \frac{dV_b}{dt}$$

Using assumption 3 ,

$$\frac{dm_b}{dt} = \frac{V_b \; \rho_b}{\gamma_b \; P} \frac{dP}{dt} + \rho_b \frac{dV_b}{dt} \qquad (A)$$

To solve for the second term of equation A,

$$\frac{\rho_b}{\rho_u} \frac{dm_u}{dt} = (V_o - V_b) \; \frac{\rho_b}{\gamma_u \; P} \frac{dP}{dt} - \rho_b \frac{dV_b}{dt}$$

$$\rho_b \frac{dV_b}{dt} = (V_o - V_b) \; \frac{\rho_b}{\gamma_u \; P} \frac{dP}{dt} + \frac{\rho_b}{\rho_u} \frac{dm_b}{dt} \qquad (B)$$

61

Substituting (B) into (A) and simplifying,

$$\frac{dm_b}{dt} = \frac{1}{\left(1 - \frac{\rho_b}{\rho_u}\right)} \left[\frac{m_o(P-P_o)}{(P_{cv}-P_o)} \left(\frac{1}{\gamma_b} - \frac{1}{\gamma_u} \right) + \frac{V_o \rho_b}{\gamma_u} \right] \frac{1}{P} \frac{dP}{dt}$$

But ρ_b is not constant during the burn. Using assumptions 2 and 4, the burning rate equation becomes,

$$\frac{dm_b}{dt} = \frac{\rho_u}{\left(\rho_u - \rho_{b,o} \left[\frac{P}{P_o}\right]^{\frac{1}{\gamma_b}}\right)} \left[\frac{m_o(P-P_o)}{(P_{cv}-P_o)} \left(\frac{1}{\gamma_b} - \frac{1}{\gamma_u} \right) + \frac{V_o \rho_{b,o} \left[\frac{P}{P_o}\right]^{\frac{1}{\gamma_b}}}{\gamma_u} \right] \frac{1}{P} \frac{dP}{dt}$$

The burning velocity, S_T, is related to the burning rate by the following,

$$S_T = \frac{1}{\rho_u A_f} \frac{dm_b}{dt}$$

62

The area of the flame can be calculated using assumptions 1 and 2, giving

$$A_f = (36\pi)^{\frac{1}{3}} \left(\frac{m_o}{\rho_{b,o} \left[\frac{P}{P_o} \right]^{\frac{1}{\gamma_b}}} * \frac{P-P_o}{\Delta P_{cv}} \right)^{\frac{2}{3}}$$

This gives the equation for the burning velocity,

$$S_T = \frac{1}{\rho_u} (36\pi)^{-\frac{1}{3}} \left(\frac{m_o}{\rho_{b,o} \left[\frac{P}{P_o} \right]^{\frac{1}{\gamma_b}}} \frac{P-P_o}{\Delta P_{cv}} \right)^{-\frac{2}{3}} \frac{dm_b}{dt}$$

The equations for the burning rate and burning velocity can be solved by measuring the pressure and the slope of the pressure trace (P and dP/dt). The remaining numbers are constant for a given concentration of hydrogen, steam, and air.

APPENDIX C: Listing of data analysis program

MAIN PROGRAM

```
      PROGRAM Power Spectrum
      INCLUDE 'STDHDR.FOR'
      REAL*8
MAXVOLT,MINVOLT,SU,SV,UAV,VAV,RMSU,RMSV,SKU,SKV,FLU,FLV
      REAL*8 UV,RMSUV,DMAXV,DKBYTES,TRANS
      REAL*8 U(0:MAXV)
      REAL XIMAG(0:MAXV),POWER(0:MAXV),XREAL(0:MAXV)
      REAL INTERVAL,C1,C2
      REAL STEP1,STEP2
      REAL*8 D1,D2,V
      REAL QC(49,23), GC(49,23),E1(49), E2(49,23)
      INTEGER*2 ID1,ID2
      INTEGER I,F,J,NS,NE1,NE2,Z,P,M,KBYTES,L,W,MAXF,PSYN,B
      CHARACTER*40 FNAME,ONAME,PSNAME
C
      DMAXV = DFLOAT(MAXV)
      W = 2
C
C  Read in calibration table
C
      OPEN(UNIT=1,FILE="CALIB.DAT")
      READ(1,15) STEP1
      READ(1,15) STEP2
      READ(1,14) NE1
      READ(1,14) NE2
      DO 10 I=1,NE1
        DO 11 J=1,NE2
          READ(1,*,END=16) E1(I),E2(I,J),QC(I,J),GC(I,J)
11        CONTINUE
10      CONTINUE
C
14      FORMAT(I4)
15      FORMAT(F6.1)
16      CLOSE (UNIT = 1)
C
C   Read in information from input file
      OPEN (UNIT=9,FILE="LISTPS.DAT")
C   Read in the number of files
      READ(9,*) P
      DO 999 Z=0,P-1
      READ(9,1004) FNAME
      WRITE(*,1001) FNAME
```

```fortran
      READ(9,1004) ONAME
      WRITE(*,1005) ONAME
      READ(9,1) PSYN
1     FORMAT(I4)
      IF(PSYN.EQ.1) READ(9,1004) PSNAME
      IF(PSYN.EQ.1) WRITE(*,1007) PSNAME
      READ(9,2) KBYTES,M,MAXF,C1,C2
2     FORMAT(I4,2X,I4,2X,I8,2X,F5.2,2x,F5.2)
      WRITE(*,1003)  MAXF/1000.0
      WRITE(*,1000)  KBYTES
      WRITE(*,1006)  M
      WRITE(*,1002)  C1
      WRITE(*,1008)  C2
      INTERVAL = 1.0D0 / MAXF
      MAXF = MAXF
      KBYTES = KBYTES / (MAXV / 1024)
      DKBYTES = DFLOAT(KBYTES)
      IF(M.LT.1536) M=1024
      IF(M.GT.3072) M=4096
      IF(M.GE.1536.AND.M.LE.3072) M=2048
      M=2*M
C
C   Read in anemometer data, checking channel tag.
C
      OPEN(UNIT=3,FILE=FNAME,form='binary')
C
C
      SU=0.0D0
      SV=0.0D0
      UAV = 0.0D0
      VAV = 0.0D0
      RMSU = 0.0D0
      RMSV = 0.0D0
      RMSUV = 00D0
      SKU = 0.0D0
      SKV = 0.0D0
      FLU = 0.0D0
      FLV = 0.0D0
      UV = 0.0D0
      MINVOLT = 1D+30
      MAXVOLT = -1D+30
      NS=0
      B=0
C
```

```
C
C   This loop accumulates the data, converting to velocities
C

      OPEN(4,FILE=ONAME)
      DO 90 L=1,KBYTES
      DO 40 I=1,MAXV
      F=1
        READ(3) ID2,ID1
      ID1=ISHFT(ID1,-4)
      ID2=ISHFT(ID2,-4)
      IF(ID1.LT.0) ID1=ID1+4096
      IF(ID2.LT.0) ID2=ID2+4096
      D1=4.88281D-3*DFLOAT(ID1-2048)
      D2=4.88281D-3*DFLOAT(ID2-2048)
      D1=D1*C1
      D2=D2*C2
C
C   This subroutine uses a lookup table to convert the data to velocities.
C
      CALL LOOK(I,F,STEP1,STEP2,NE1,NE2,
     *         D1,D2,E1,E2,QC,GC,U(I),V)
      IF (F.EQ.0) B=B+1
      IF (F.EQ.0) GOTO 40
      NS=NS+1
      IF (U(I).LE.MAXVOLT) GOTO 45
      MAXVOLT = U(I)
45    CONTINUE
      IF (U(I).GE.MINVOLT) GOTO 46
      MINVOLT = U(I)
46    CONTINUE
C
C   Here the velocities are accumulated.
C
C     XDATA(NS)=U(I)
      SU = SU + U(I)
      SV = SV + V
      UV = UV + U(I)*V
      RMSU=RMSU+U(I)*U(I)
      RMSV=RMSV+V*V
      SKU=SKU+U(I)**3
      SKV=SKV+V**3
      FLU=FLU+U(I)**4
      FLV=FLV+V**4
40    CONTINUE
```

67

```fortran
      IF(PSYN.EQ.1) THEN
        DO 50 I=0,M-1
          POWER(I)=0.0D0
50      CONTINUE
        J=1
60      CONTINUE
        DO 70 I=0,M-1
          XREAL(I)=U(J)
          XIMAG(I)=0.0D0
          J=J+1
70      CONTINUE
        CALL WindowFFTData(XREAL, XIMAG, M, W)
        CALL PowerSpectrumCalc(XREAL, XIMAG, M, INTERVAL)
        DO 80 B=0,M-1
          POWER(B) = POWER(B) + XREAL(B)
80      CONTINUE
        IF((J+M).LT.MAXV) GO TO 60
      END IF
90    CONTINUE
91    CLOSE (UNIT = 3)
C
C   Here the average and RMS values are calculated.
C
      UAV = SU / FLOAT(NS)
      VAV = SV / FLOAT(NS)
      RMSU = RMSU / FLOAT(NS)
      RMSV = RMSV /FLOAT(NS)
      SKU = SKU / FLOAT(NS)
      SKV = SKV / FLOAT(NS)
      FLU = FLU / FLOAT(NS)
      FLV = FLV / FLOAT(NS)
      UV=UV/FLOAT(NS)-UAV*VAV
      RMSU=RMSU-UAV*UAV
      RMSV=RMSV-VAV*VAV
      SKU=SKU-UAV**3-3.0D0*UAV*RMSU
      SKV=SKV-VAV**3-3.0D0*VAV*RMSV
      FLU=FLU-UAV**4-6.0D0*UAV**2*RMSU-4.0D0*UAV*SKU
      FLV=FLV-VAV**4-6.0D0*VAV**2*RMSV-4.0D0*VAV*SKV
      RMSUV=DSQRT(RMSU*RMSV)
      UV=UV/RMSUV
      RMSU = DSQRT(RMSU)
      RMSV = DSQRT(RMSV)
      SKU=SKU/(RMSU**3)
      SKV=SKV/(RMSV**3)
```

```
      FLU=FLU/(RMSU**4)
      FLV=FLV/(RMSV**4)
C
C Here the output is written to the screen
C
      WRITE(*,1017) UAV,VAV,RMSU,RMSV,SKU,SKV,FLU,FLV,UV,
     *          MINVOLT,MAXVOLT,NS,B
      IF(PSYN.EQ.1) THEN
        TRANS = DKBYTES * DFLOAT(MAXV / M)
        DO 100 I=0,M-1
        POWER(I) = POWER(I) / TRANS
100     CONTINUE
      END IF
      M = M / 2
C
C   Here the output is saved to a file.
C
      KBYTES=KBYTES*(MAXV/1000)
      WRITE(4,1001)  FNAME
      WRITE(4,1017)  UAV,VAV,RMSU,RMSV,SKU,SKV,FLU,
     *          FLV,UV,MINVOLT,MAXVOLT,NS,B
      WRITE(4,1003)  MAXF/1000.0
      WRITE(4,1000)  KBYTES
      WRITE(4,1006)  M
      WRITE(4,1002)  C1
      WRITE(4,1008)  C2
      CLOSE (4)
      IF(PSYN.EQ.1) THEN
        OPEN (UNIT=5,FILE=PSNAME)
        WRITE(5,1001) FNAME
        WRITE(5,1010)
        DO 150 I=0,M-1
        WRITE(5,1011) XIMAG(I),POWER(I)
150     CONTINUE
        CLOSE (5)
      END IF
C
999   CONTINUE
C
C   Format statements
C
1017  FORMAT(' 'f12.6,'        Average U-velocity '/' ',
     *             f12.6,'        Average V-velocity '/' ',
     *             f12.6,'        RMSU value        '/' ',
```

69

```
*               f12.6,'        RMSV value        '/' ',
*               f12.6,'        U-Skewness factor '/' ',
*               f12.6,'        V-Skewness factor '/' ',
*               f12.6,'        U-Flatness factor '/' ',
*               f12.6,'        V-Flatness factor '/' ',
*               f12.6,'        uv correlation coeff.'/' ',
*               f12.6,'        Minimum U-value  '/' ',
*               f12.6,'        Maximum U-value  '/' ',
*     I12,'        Number of good data '/' ',
*     I12,'        Number of bad data '/' ')
1000  FORMAT(' Number of 1024 sample blocks   ',I4)
1001  FORMAT(' 'A35)
1002  FORMAT(' Correction factor(E1)=      ',F4.2)
1008  FORMAT(' Correction factor(E2)=      ',F4.2)
1003  FORMAT(' Sampling rate(kHz)=      ',F8.2)
1004  FORMAT(A40)
1005  FORMAT(' Output filename=   ',A35)
1006  FORMAT(' Number of spectral lines=    ',I4)
1007  FORMAT(' Power spectrum filename=   ',A35)
1009  FORMAT(' ',1X,f10.5,2X,F12.6)
1010  FORMAT(' ','     f     ','   u''(f)   ')
1011  FORMAT(' ',1X,G12.5,2X,G12.6)
C
      STOP
      END
```

CONVERSION SUBROUTINE (LOOK.FOR)

```
          SUBROUTINE LOOK(I,F,STEP1,STEP2,NE1,NE2,
     *               D1,D2,E1,E2,QC,GC,U,V)
          REAL    STEP1,STEP2,MTCH1,MTCH2,F1,F2,F22
          REAL    E1(49), E2(49,23)
          REAL    QC(49,23), GC(49,23)
          REAL*8  U,V,Q1,G1,Q,G,D1,D2,PI
C         CHARACTER*40 INFILE(5),OUTFILE
          INTEGER A,B,C,K,NE1,NE2,I,F
          PARAMETER ( pi=3.141592635897932)
C
C
C   This loop converts voltages to velocities using the calibration
C   table and interpolating where necessary. By matching D1 to E1 and
C   D2 to E2, the appropriate counters (A,B) are found that indicate
C   location of Q (flow rate) and G (flow angle).
C
C
C   Find match in E1(A) for D1
C
          A=1
          DO 10 K=1,NE1
          IF(E1(A).GE.D1) THEN
             MTCH1=E1(A)-D1
             A=A+1
          END IF
10        CONTINUE
          A=A-1
          STEP1=E1(A+1)-E1(A)
          F1=MTCH1/STEP1
          IF(E1(NE1).EQ.D1) THEN F1=0.0D0
C
C   If F1<>0, will need to interpolate between E1(A) and E1(A+1).
C   But first, find match in E2 for D2(I)
C
          B=1
          DO 20 K=1,NE2
          IF(E2(A,B).LE.D2) THEN
             MTCH2=D2-E2(A,B)
             B=B+1
          END IF
20        CONTINUE
          B=B-1
```

```
      STEP2=E2(A,B+1)-E2(A,B)
      F2=MTCH2/STEP2
      IF(E2(A,NE2).EQ.D2) THEN F2=0.0D0
      IF(B.EQ.NE2.AND.E2(A,NE2).LT.D2) THEN
         F=0
         WRITE(4,*) 'Voltage out of range: E2(A,NE2)'
         WRITE(4,*) 'I= ',I,' D1= ',D1,' D2= ',D2
         GOTO 299
      ELSE IF(B.EQ.0.AND.E2(A,1).GT.D2) THEN
         F=0
         WRITE(4,*) 'Voltage out of range: E2(A,1)'
         WRITE(4,*) 'I= ',I,' D1= ',D1,' D2= ',D2
         GOTO 299
      END IF


C
C   If F2<>0, will need to interpolate between E2(A,B) and E2(A,B+1).
C   This will be done using Q1,G1 .
C
      IF(F2.EQ.0) THEN
         Q1=QC(A,B)
         G1=GC(A,B)
      ELSE
         Q1=(QC(A,B+1)-QC(A,B))*F2+QC(A,B)
         G1=(GC(A,B+1)-GC(A,B))*F2+GC(A,B)
      END IF
C
C   If F1<>0, need to find E2(A+1,C) for further interpolation, unless
C   A+1=NE2: in this case set C=5(arbitrarily)
C
      IF(A+1.LT.NE1) THEN
      C=1
      DO 30 K=1,NE2
      IF(E2(A+1,C).LE.D2) THEN
         MTCH2=D2-E2(A+1,C)
         C=C+1
      END IF
30    CONTINUE
      C=C-1
      STEP2=E2(A+1,C+1)-E2(A+1,C)
      F22=MTCH2/STEP2
      IF(E2(A+1,NE2).EQ.D2) THEN F22=0.0D0
      IF(C.EQ.NE2.AND.E2(A+1,NE2).LT.D2) THEN
         F=0
```

72

```
            WRITE(4,*) 'Voltage out of range: E2(A+1,NE2)'
            WRITE(4,*) 'I= ',I,' D1= ',D1,' D2= ',D2
            GOTO 299
          ELSE IF(C.EQ.0.AND.E2(A+1,1).GT.D2) THEN
            F=0
            WRITE(4,*) 'Voltage out of range: E2(A+1,1)'
            WRITE(4,*) 'I= ',I,' D1= ',D1,' D2= ',D2
            GOTO 299
          END IF
        ELSE IF(A+1.EQ.NE2) THEN
            MTCH2=0.0D0
            C=5
        END IF
C
C    If F22<>0, will need to interpolate between E2(A+1,C) and E2(A+1,C+1).
C    This will be done using  Q2,G2.
C
C    Now have Q1, G1 at E1(A) and at E2(A,B) or between E2(A,B+1) and E2(A,B)
C    If E1(A) matched D1(I) exactly, then no interpolation with Q2,G2 is needed.
C
        IF(F1.EQ.0) THEN
            Q=Q1
            G=G1
        ELSE
C
C        otherwise, need to interpolate between E1(A+1),E2a and E1(A),E2b
C        Get Q2, G2 at E1(A+1), E2b
C        (where E2b is E2(A+1,C) or between E2(A+1,C) and E2(A+1,C+1))
C
            IF(MTCH2.EQ.0) THEN
                Q2=QC(A+1,C)
                G2=GC(A+1,C)
            ELSE
                Q2=(QC(A+1,C+1)-QC(A+1,C))*F22+QC(A+1,C)
                G2=(GC(A+1,C+1)-GC(A+1,C))*F22+GC(A+1,C)
            END IF
C
C        Now interpolate between Q1,Q2 and G1,G2
C
            Q=(Q2-Q1)*F1+Q1
            G=(G2-G1)*F1+G1
        END IF
C
C    Convert the flow rate and flow angle to U and V velocities
```

73

```
C
      U=Q*COS(G*pi/180)
      V=Q*SIN(G*pi/180)
C
210   CONTINUE
c     IF(A.GE.40.OR.B.GE.12.OR.C.GE.12) THEN
C      WRITE(4,*) ' I = ',I
C      WRITE(4,*) ' A = ',A,' B = ',A,' C = ',C
C      WRITE(4,*) ' Q = ',Q,'  G = ',G
C      WRITE(4,*) ' U = ',U,'  V = ',V
C      WRITE(4,*) ' D1 = ',D1,'  D2 = ',D2
c     END IF
C     write(*,*) 'end of loop'
C
299   CONTINUE
C
      RETURN
      END
```

POWER SPECTRUM SUBROUTINE

This subroutine is taken from [34] under the name **FFT.FOR**.

INCLUDE FILE STDHDR.FOR

```
INTEGER maxv,maxr,maxc
REAL pi
PARAMETER (maxc = 10)
PARAMETER (maxv = 8192)
PARAMETER (maxr = 30)
PARAMETER (pi = 3.141592635897932)
```